

NASA/CR-2002-211958



# Finite Element *A Posteriori* Error Estimation for Heat Conduction

*Christopher G. Lang*  
*The George Washington University*  
*Joint Institute for Advancement of Flight Sciences*  
*Langley Research Center, Hampton, Virginia*

---

November 2002

## The NASA STI Program Office ... in Profile

Since its founding, NASA has been dedicated to the advancement of aeronautics and space science. The NASA Scientific and Technical Information (STI) Program Office plays a key part in helping NASA maintain this important role.

The NASA STI Program Office is operated by Langley Research Center, the lead center for NASA's scientific and technical information. The NASA STI Program Office provides access to the NASA STI Database, the largest collection of aeronautical and space science STI in the world. The Program Office is also NASA's institutional mechanism for disseminating the results of its research and development activities. These results are published by NASA in the NASA STI Report Series, which includes the following report types:

- **TECHNICAL PUBLICATION.** Reports of completed research or a major significant phase of research that present the results of NASA programs and include extensive data or theoretical analysis. Includes compilations of significant scientific and technical data and information deemed to be of continuing reference value. NASA counterpart of peer-reviewed formal professional papers, but having less stringent limitations on manuscript length and extent of graphic presentations.
- **TECHNICAL MEMORANDUM.** Scientific and technical findings that are preliminary or of specialized interest, e.g., quick release reports, working papers, and bibliographies that contain minimal annotation. Does not contain extensive analysis.
- **CONTRACTOR REPORT.** Scientific and technical findings by NASA-sponsored contractors and grantees.

- **CONFERENCE PUBLICATION.** Collected papers from scientific and technical conferences, symposia, seminars, or other meetings sponsored or co-sponsored by NASA.
- **SPECIAL PUBLICATION.** Scientific, technical, or historical information from NASA programs, projects, and missions, often concerned with subjects having substantial public interest.
- **TECHNICAL TRANSLATION.** English-language translations of foreign scientific and technical material pertinent to NASA's mission.

Specialized services that complement the STI Program Office's diverse offerings include creating custom thesauri, building customized databases, organizing and publishing research results ... even providing videos.

For more information about the NASA STI Program Office, see the following:

- Access the NASA STI Program Home Page at <http://www.sti.nasa.gov>
- E-mail your question via the Internet to [help@sti.nasa.gov](mailto:help@sti.nasa.gov)
- Fax your question to the NASA STI Help Desk at (301) 621-0134
- Phone the NASA STI Help Desk at (301) 621-0390
- Write to:  
NASA STI Help Desk  
NASA Center for AeroSpace Information  
7121 Standard Drive  
Hanover, MD 21076-1320

NASA/CR-2002-211958



# Finite Element *A Posteriori* Error Estimation for Heat Conduction

*Christopher G. Lang*  
*The George Washington University*  
*Joint Institute for Advancement of Flight Sciences*  
*Langley Research Center, Hampton, Virginia*

National Aeronautics and  
Space Administration

Langley Research Center  
Hampton, Virginia 23681-2199

Prepared for Langley Research Center  
under Cooperative Agreement NCC1-01017

---

November 2002

---

Available from:

NASA Center for AeroSpace Information (CASI)  
7121 Standard Drive  
Hanover, MD 21076-1320  
(301) 621-0390

National Technical Information Service (NTIS)  
5285 Port Royal Road  
Springfield, VA 22161-2171  
(703) 605-6000

## Abstract

This research investigates residual-based *a posteriori* error estimates for finite element approximations of heat conduction in single-layer and multi-layered materials. The finite element approximation is based upon hierarchical modelling combined with p-version finite elements. Hierarchical modelling results in thermal elements which are geometrically compatible with structural finite elements. Thermal stresses are an important concern when designing reusable launch vehicles, and accurate temperature distributions throughout the structure are required.

*A posteriori* error estimation is a way to determine the accuracy of an approximate thermal solution when the exact solution is unknown. Error estimates are also necessary for developing an adaptive scheme which is the automatic process of mesh refinement and p-enrichment to deliver a solution with the desired accuracy.

Element error indicators are determined by solving an element equation for the error using the element residual, and a global error estimate in the energy norm is computed by collecting the element contributions. Two methods, the average flux and the equilibrated flux method, are discussed for constructing the element flux boundary condition for the error equation. The error estimation is extended to multi-layered materials, and a directional error indicator is developed to distinguish the error in the hierarchical model from the error in the finite element method. Comparisons of the actual and estimated error show that the equilibrated flux method provides accurate estimates of the error for single and multi-layered materials. Numerical results also show that the directional indicators accurately determine which contribution to the total error dominates. This is an essential step in implementing an effective adaptive scheme.

## **Acknowledgements**

First, I would like to thank Dr. Kim S. Bey from the Metals and Thermal Structures Branch at NASA Langley Research Center. Her extensive knowledge and support was invaluable for this thesis. I would also like to thank Dr. Paul Cooper for his advice and guidance throughout the completion of this project and Dr. Stephen Scotti for the opportunity to perform research at the Metals and Thermal Structures Branch. Last but not least, I would like to thank my family for the love and support that they have always given me.

# Contents

|          |   |           |
|----------|---|-----------|
| <b>1</b> | <b>Introduction</b>   | <b>1</b>  |
| 1.1      | Background . . . . .  | 1         |
| 1.2      | Review of Previous Research . . . . .                         | 4         |
| 1.3      | Purpose . . . . .   | 5         |
| 1.4      | Scope . . . . .   | 6         |
| <b>2</b> | <b>Finite Element Thermal Analysis</b>                        | <b>7</b>  |
| 2.1      | Boundary Value Problem for Conduction Heat Transfer . . . . . | 8         |
| 2.2      | Weak Formulation . . . . .                                    | 10        |
| 2.3      | Finite Element Method . . . . .                               | 11        |
| 2.3.1    | Hierarchical Modelling . . . . .                              | 12        |
| 2.3.2    | P-Element Approximation . . . . .                             | 15        |
| 2.3.3    | Element Matrices . . . . .                                    | 18        |
| 2.3.4    | Global System of Equations . . . . .                          | 20        |
| <b>3</b> | <b>A Posteriori Error Estimation</b>                          | <b>23</b> |
| 3.1      | Element Residual Method . . . . .                             | 24        |
| 3.2      | Element Boundary Conditions . . . . .                         | 26        |
| 3.2.1    | Average Element Boundary Flux . . . . .                       | 27        |
| 3.2.2    | Equilibrated Flux . . . . .                                   | 28        |
| 3.3      | Error Indicator . . . . .                                     | 33        |

|          |  |           |
|----------|--|-----------|
| 3.4      | Numerical Examples for the Total Error . . . . .                 | 35        |
| 3.4.1    | Case I: Smooth Solution . . . . .                                | 36        |
| 3.4.2    | Case II: Rough Solution . . . . .                                | 41        |
| 3.5      | Directional Error Indicators . . . . .                           | 47        |
| 3.6      | Numerical Examples for the Directional Error Estimates . . . . . | 50        |
| <b>4</b> | <b>Extension to Multi-layered Materials</b>                      | <b>53</b> |
| 4.1      | Boundary Value Problem . . . . .                                 | 53        |
| 4.2      | Finite Element Method for Multi-Layers . . . . .                 | 54        |
| 4.2.1    | Weak Formulation . . . . .                                       | 55        |
| 4.2.2    | Optimal Hierarchical Model . . . . .                             | 55        |
| 4.2.3    | Element Equations . . . . .                                      | 56        |
| 4.3      | Multi-Layer <i>A Posteriori</i> Error Estimation . . . . .       | 58        |
| 4.3.1    | Element Residual Method . . . . .                                | 58        |
| 4.3.2    | Equilibrated Boundary Flux Approximation . . . . .               | 59        |
| 4.3.3    | Multi-Layer Error Indicator . . . . .                            | 61        |
| 4.4      | Numerical Examples . . . . .                                     | 62        |
| <b>5</b> | <b>Concluding Remarks</b>  | <b>67</b> |
| 5.1      | Summary . . . . .  | 67        |
| 5.2      | Conclusions . . . . .  | 68        |
| 5.3      | Recommendations . . . . .  | 68        |

# List of Figures

|      |  |    |
|------|--|----|
| 2.1  | Two-dimensional domain $\Omega$ for an orthotropic material. . . . .   | 9  |
| 2.2  | Discretization of the domain for the finite element method. . . . .  | 13 |
| 2.3  | One-dimensional (a) quadratic Lagrange element and (b) cubic Lagrange element with corresponding basis functions. . . . .        | 16 |
| 2.4  | Element basis functions, $\phi$ and $\psi$ , for $p = 1$ through 7. . . . .  | 17 |
| 3.1  | Convention for node and edge labels for an expanded local element. . . . .   | 30 |
| 3.2  | First four two-dimensional basis functions for edge $\gamma_2$ . . . . .   | 31 |
| 3.3  | Two-dimensional plate for numerical examples. . . . .  | 36 |
| 3.4  | Exact solution for Case I. . . . .   | 37 |
| 3.5  | Error for Case I using the average flux method. . . . .  | 39 |
| 3.6  | Error for Case I using the equilibrated flux method. . . . .   | 40 |
| 3.7  | Exact solution for Case II. . . . .  | 42 |
| 3.8  | Error for Case II using the average flux method. . . . .   | 43 |
| 3.9  | Error for Case II using the equilibrated flux method. . . . .  | 44 |
| 3.10 | Pointwise error in the finite element solution for Case II using 32 elements with $p_x = p_z = 2$ . . . . .                      | 45 |
| 3.11 | Element error indicators for Case II solution using 32 elements with $p_x = p_z = 2$ using the average flux method. . . . .      | 46 |
| 3.12 | Element error indicators for Case II solution using 32 elements with $p_x = p_z = 2$ using the equilibrated flux method. . . . . | 46 |

|      |  |    |
|------|--|----|
| 3.13 | Directional error estimation for Case I using the equilibrated flux method.  | 51 |
| 3.14 | Directional error estimation for Case II using the equilibrated flux method. . . . .                                     | 52 |
| 4.1  | Two-dimensional domain for a multi-layered material. . . . .   | 54 |
| 4.2  | The optimal basis functions for a three layer material with $(k_z)_1 = 1$ , $(k_z)_2 = 10$ , and $(k_z)_3 = 1$ . . . . . | 57 |
| 4.3  | Example of a discontinuous exact boundary flux in the $x$ -direction on a four layer element. . . . .                    | 59 |
| 4.4  | Two-dimensional plate with two layers for numerical results. . . . .   | 62 |
| 4.5  | Exact solution for the two layer example. . . . .  | 63 |
| 4.6  | Actual error in solutions obtained for two layer example. . . . .  | 65 |
| 4.7  | Comparison of the actual and estimated error for the two layer example.  | 66 |

# Nomenclature

| <u>Symbol</u>           | <u>Definition</u>  |
|-------------------------|--|
| $a, b, c$               | constant coefficients  |
| $\mathbf{a}$            | global nodal unknowns  |
| $\mathbf{a}_e$          | element nodal unknowns   |
| $d$                     | thickness of domain in the $z$ -direction                        |
| $e$                     | total error in finite element solution, $e = e_{Model} + e_{FE}$ |
| $e_{FE}$                | error in finite element approximation                            |
| $e_{Model}$             | error in hierarchical model                                      |
| $\hat{e}$               | estimated error, approximation to $e$                            |
| $   f   $               | energy norm of the function $f$                                  |
| $h$                     | mesh size in the $x$ -direction                                  |
| $i, j$                  | index  |
| $k_{ij}$                | component of thermal conductivity tensor $\boldsymbol{\kappa}$   |
| $k_x$                   | thermal conductivity in $x$ -direction                           |
| $k_z$                   | thermal conductivity in $z$ -direction                           |
| $(k_x)_i$               | thermal conductivity of layer $i$ in $x$ -direction              |
| $(k_z)_i$               | thermal conductivity of layer $i$ in $z$ -direction              |
| $n_L$                   | total number of layers   |
| $\mathbf{n}_{\Omega^e}$ | normal vector to element $\Omega^e$                              |
| $n_\gamma$              | number of nodal basis functions along an edge                    |

|                      |  |
|----------------------|--|
| $p_x$                | order of approximation in the $x$ -direction                 |
| $p_z$                | order of approximation in the $z$ -direction                 |
| $\mathbf{q}$         | heat flux vector   |
| $q_b$                | normal heat flux applied to bottom boundary of plate         |
| $q_s$                | normal heat flux applied to Neumann boundary                 |
| $q_t$                | normal heat flux applied to top boundary of plate            |
| $\hat{q}$            | approximate element boundary flux for error estimate         |
| $\bar{q}$            | average element boundary flux                                |
| $\tilde{q}$          | deviation of equilibrated flux from average flux             |
| $q_0$                | constant coefficient for heat load                           |
| $s$                  | coordinate along a boundary                                  |
| $u$                  | temperature, exact solution to heat conduction equation      |
| $u_{Model}$          | exact solution to the hierarchical model                     |
| $u_s$                | constant temperature on Dirichlet boundary                   |
| $\hat{u}$            | approximate temperature solution                             |
| $v$                  | test function  |
| $\hat{v}$            | approximate test function                                    |
| $x, y, z$            | Cartesian coordinates  |
| $x_0$                | $x$ -coordinate of left node of an element                   |
| $x_1$                | $x$ -coordinate of right node of an element                  |
| $z_i$                | $z$ -coordinate of top edge of material layer $i$            |
| $\mathbf{A}$         | general $(n \times n)$ matrix                                |
| $A_{ij}$             | component of matrix $\mathbf{A}$                             |
| $A_n, B_n, C_n, D_n$ | Fourier coefficients of exact solution term; function of $n$ |
| $\mathbf{B}$         | general $(m \times m)$ matrix                                |
| $B_{ij}$             | component of matrix $\mathbf{B}$                             |

|                          |   |
|--------------------------|---|
| $B(\cdot, \cdot)$        | bilinear functional                                   |
| $C$                      | coefficient used in penalty method                    |
| $F(\cdot)$               | linear functional associated with source term         |
| $H^1(\Omega)$            | Hilbert space   |
| $\mathbf{K}$             | stiffness matrix                                      |
| $L$                      | length of domain in the $x$ -direction                |
| $L(\cdot)$               | linear functional                                     |
| $\mathbf{M}$             | mass matrix   |
| $N_{el}$                 | total number of elements in a mesh                    |
| $N_i$                    | shape function  |
| $P_i$                    | Legendre polynomial of degree $i$                     |
| $Q$                      | internal heat source                                  |
| $R(\cdot)$               | residual functional                                   |
| $V(\Omega)$              | infinite dimensional subspace of $H^1(\Omega)$        |
| $\hat{V}(\Omega)$        | finite dimensional subspace of $V(\Omega)$            |
| $\alpha$                 | constant parameter                                    |
| $\boldsymbol{\alpha}$    | vector of constant coefficients for equilibrated flux |
| $\alpha_n^i$             | exact solution term; function of $n$ for layer $i$    |
| $\gamma$                 | element edge  |
| $\Gamma_D$               | Dirichlet boundary                                    |
| $\Gamma_N$               | Neumann boundary                                      |
| $\delta_{mn}$            | Kronecker delta                                       |
| $\eta$                   | local coordinate in $z$ -direction                    |
| $\varepsilon$            | global error indicator                                |
| $\varepsilon_{\Omega^e}$ | element error indicator                               |
| $\varepsilon_{FE}$       | finite element error indicator                        |

|                              |  |
|------------------------------|--|
| $\varepsilon_{Model}$        | hierarchical modelling error indicator                                   |
| $\boldsymbol{\theta}$        | vector of two-dimensional element basis functions                        |
| $\theta_n$                   | two-dimensional basis function for node $n$                              |
| $\boldsymbol{\theta}^\gamma$ | vector of two-dimensional basis functions along edge $\gamma$            |
| $\theta_n^\gamma$            | two-dimensional basis function for node $n$ along edge $\gamma$          |
| $\boldsymbol{\kappa}$        | thermal conductivity tensor  |
| $\xi$                        | local coordinate in $x$ -direction                                       |
| $\rho c_p$                   | heat capacity  |
| $\sigma$                     | increased order of error approximation                                   |
| $\phi$                       | element basis functions in $x$ -direction                                |
| $\boldsymbol{\chi}$          | element basis functions, outer tensor product of $\phi$ and $\psi$       |
| $\hat{\boldsymbol{\chi}}$    | element basis functions, outer tensor product of $\phi$ and $\hat{\psi}$ |
| $\psi$                       | element basis functions in $z$ -direction                                |
| $\hat{\psi}$                 | optimal through-thickness basis functions for multi-layered materials    |
| $\Omega$                     | domain   |
| $\Omega^e$                   | element domain   |
| $\Omega^{e'}$                | neighboring element domain   |
| $\partial\Omega^e$           | boundary of element $\Omega^e$   |
| $\partial\Omega^{e'}$        | boundary of neighboring element $\Omega^{e'}$                            |
| <b><u>Operator</u></b>       | <b><u>Definition</u></b>   |
| $\otimes$                    | outer tensor product   |
| $\nabla$                     | gradient vector  |
| $\cap$                       | intersection   |

# Chapter 1

## Introduction

When performing structural analysis of hot structures, it is necessary to understand the temperature distribution throughout the structure. Thermal concerns include maximum and minimum temperatures, thermal stresses induced by temperature gradients, and rates of heat flow depending on the application of the material being studied. Therefore, efficient and dependable methods of computing thermal solutions are vital in the design and analysis of thermal structures. For example, reusable launch vehicles must be able to repeatedly withstand the extreme temperatures present during Earth re-entry. The Thermal Protection System (TPS) is the primary outer material that protects the system from high temperatures. Materials and concepts are continuously being investigated to improve the insulating properties for TPS. Such multi-layered materials include composite laminates and TPS panels composed of insulation between two layers of metal to replace the tiles used on the orbiter of the Space Shuttle system. Therefore, the numerical analysis of these types of materials, along with error estimates, will aid in the design process.

### 1.1 Background

The finite element method is a popular numerical analysis tool for engineers working thermal problems with complex geometry or boundary conditions. The advances in

finite element approaches and computer technology have increased the usefulness of finite element methods and allowed for more accurate and efficient approximations. One such advanced method is the hierarchical p-version finite element method. The use of hierarchical modelling allows the dimension of the domain to be reduced by one dimension. The benefit of this approach is that mesh regeneration is not required when changing the approximation order to obtain a more accurate solution.

When making numerical approximations with the finite element method, it is useful to know how accurately the methods approximate the exact solution. Error estimation is widely known and used to answer the question, 'How good is the finite element solution?' Knowledge of the application of the problem and an understanding of how the error behaves can reduce the computational effort needed to achieve the desired accuracy.

The two types of error estimates are *a priori* and *a posteriori*. *A priori* error estimates contain the exact solution and the parameters that influence the accuracy of the approximate solution. This type of error estimate provides information on the convergence and stability of the method and gives the asymptotic behavior of the error in the approximation as mesh size and polynomial orders are appropriately varied [1].

The second type is *a posteriori* error estimates, that are computed from the finite element approximation and the given problem data and do not require the exact solution to the problem. Since approximation methods are generally used because the exact solution is not known for a the problem of interest, *a posteriori* error estimates are useful for determining accuracy when analyzing complex problems for which the solution is unknown. *A posteriori* error estimates are also necessary for adaptivity and control of the finite element approximation error. Adaptivity is a method of automatically refining the mesh or increasing the polynomial degree in particular

regions where the finite element error is greatest. These regions of large error occur near steep solution gradients, singularities, or discontinuities in applied loadings. The mesh can be refined or the polynomial degree increased in these particular areas to improve the solution instead of the costly approach of refining the entire mesh. Through the use of a tolerance, local refinements can be made after each approximate solution is obtained until the error is within a specified tolerance, and this repeating method can be done with no further input from the analyst. Therefore the method can be set up and allowed to continue without any further input from the analyst. Accurate *a posteriori* error estimates are essential to the success of such an adaptive procedure.

The two main categories of *a posteriori* error estimates are explicit and implicit. Explicit error estimates involve a direct computation (usually post-processing) using the finite element solution and the given problem data and include an unknown constant which is typically ignored. Implicit error estimators involve the approximation of a boundary value problem for the error using residuals and generally involve the solution of a system of equations, and are usually more accurate than explicit error estimates [2]. Although more computational time is generally required for implicit error estimates, the improved accuracy can be worth the extra effort.

When a mesh is defined for finite element analysis, the process usually involves a combination of experience, intuition, and guesswork. If the results of the finite element approximation appear reasonable, then the solution is accepted. If not, then the mesh is redesigned. But this process is time consuming, and without an *a posteriori* error estimate, there is no other reliable and precise way of judging the acceptability of the solution except to uniformly refine the mesh until the solution converges. *A posteriori* error estimation provides the analyst with a method of measuring the quality of the computed solution. A more accurate solution can then be obtained by selecting

various parameters to change such as the value of the polynomial approximation and the mesh size locally where errors are large. For the hierarchical p-version finite element method, directional error indicators indicate which parameters will efficiently improve the solution by providing a measure of the modelling error and the finite element error separately.

## 1.2 Review of Previous Research

The hierarchical p-version finite element method was pioneered by Babuška, Szabó, and Peano in the mid to late 1970's and early 1980's [3] and [4]. Hierarchical modelling helps to simplify the problem by reducing the dimension by one before the p-version finite element method is applied. An optimal set of basis functions for the through-thickness direction that account for the piecewise continuous behavior of the solution to multi-layered problems was developed by Vogelius and Babuška in 1981 [5]. Another method for approximating the solution in multi-layered problems is the Zig-Zag method developed in 1996 by Averill and Yip [6], which uses a single polynomial approximation through the thickness with a piecewise linear function superimposed on it. The coefficients for the piecewise linear function are determined from continuity conditions at the interfaces of the layers. The optimal basis functions are used with the hierarchical p-version finite element method for multi-layered materials in this research since the use of the Zig-Zag method requires more computation when using p-enrichment for the through thickness polynomial approximation.

The subject of *a posteriori* error estimation has grown in popularity since the pioneering work of Babuška and Rheinholdt in the late 1970's. The first *a posteriori* error estimates for linear elliptic problems were developed by Babuška and Rheinholdt to guide local mesh refinement [7] and obtain accurate results without refining the entire mesh. Since then, *a posteriori* error analysis has been developed for parabolic

and hyperbolic partial differential equations. One method of *a posteriori* error estimation is the flux-projection method, which is based on the smoothing of the fluxes and comparing them with the finite element fluxes [2]. The method used in this work, called the element residual method, was first introduced in 1984 at a conference in Lisbon [8] and uses the residuals of the finite element solution. The element residual method requires element boundary conditions. One method of approximating the element boundary fluxes is the equilibrated flux method, which is based on the work by Ladeveze and Leguillon [9], Kelly [10], and Bank and Weiser [11] and is used in this research. Ainsworth and Oden advanced the element residual method using equilibrated fluxes for application to different types of problems [12].

The basic techniques for *a posteriori* error estimation were established in the early 1990's. In recent years, a new approach in the study of *a posteriori* error estimates has emerged called goal-oriented error estimation. The error is measured with respect to a specific goal of the analysis, called the quantity of interest, instead of in the energy norm, and techniques have been established to obtain upper and lower bounds of the error. This approach requires the solution of the adjoint problem, or the dual solution, to compute an influence function which relates the residual to the error in the quantity of interest [13]. Therefore, it is more computationally expensive. Currently, the emphasis is on the study of robustness of existing estimators and the identification of limits on their performance.

### 1.3 Purpose

The purpose of this research is to apply *a posteriori* error analysis to two-dimensional heat conduction for single and multi-layered materials. The three primary goals of this research are to (i) compare the results of *a posteriori* error estimates using two methods of approximating the interior boundary flux, an average flux and an equi-

librated flux, for single-layered materials, (ii) extend and examine the performance of the error estimate for multi-layered materials, and (iii) develop directional error indicators to distinguish between the modelling error and the finite element error.

## 1.4 Scope

The hierarchical p-version finite element method for solving steady state heat conduction problems is presented in Chapter 2. The weak form of the boundary value problem is developed followed by the hierarchical modelling in the through-thickness direction and the spatial p-version finite element method. Basis functions are described, and element matrices are defined. Finally, the method for enforcing the boundary conditions and solving the global system of equations are discussed.

The element residual method of *a posteriori* error estimation is discussed in Chapter 3. The derivation of the element boundary value problem for the error is presented. The element boundary conditions are discussed with two methods of approximating the interior element flux, the average flux and the equilibrated flux method. The solution for the error in the energy norm is presented next with some numerical examples. Finally directional error indicators are introduced with some numerical examples to verify the error estimates. Chapter 4 presents the application of element residual *a posteriori* error estimation to multi-layered materials. The finite element method for multi-layered materials is discussed with the choice of optimal through-thickness basis functions for hierarchical modelling. The boundary value problem for each layer is discussed followed by a discussion of the equilibrated flux method used to approximate the interior element boundary flux. Finally, some numerical examples are presented for a two layer problem. A review of the work presented in the thesis is discussed in Chapter 5. A summary of the first four chapters is presented followed by conclusions and recommendations for future work.

## Chapter 2

# Finite Element Thermal Analysis

In all but some simple cases, the exact solution of structural problems is complex and requires an approximate solution using numerical techniques. The finite element method is a powerful tool for numerically approximating the solution to a wide range of engineering problems. There are numerous methods available for constructing a finite element approximation. Traditional finite elements use linear approximations of field variables over each element. By increasing the number of elements using mesh refinement, the approximate solution converges to the exact solution. An alternative to this approach, the p-version finite element method, is to use higher-order elements, which assume a polynomial of order  $p$  for the approximation on each element. By increasing the value of  $p$ , or p-enrichment, the approximation can be improved without increasing the number of elements. The drawback to this method using conventional higher-order elements is that the mesh must be regenerated for increased values of  $p$  since the number of nodes in an element depends on  $p$ . Mesh refinement is also an option for the p-version method.

A more practical method which has been developed is the hierarchical modelling combined with p-version finite elements method. This method uses elements with a fixed number of nodes by adding more basis functions to the existing nodes when the approximation order is increased. The use of hierarchical modelling allows the

reduction by one dimension of the domain which reduces the complexity. The benefit of this approach is that when the approximation order is changed, mesh regeneration is not required. This chapter describes the hierarchical modelling combined with p-version finite elements approach used for this research to approximate the solution for a heat conduction problem with specified heat flux and temperature boundary conditions.

## 2.1 Boundary Value Problem for Conduction Heat Transfer

The goal is to solve for the temperature,  $u$ , in a built-up structure using the general heat conduction equation. According to the conservation of energy, the rate of heat entering and leaving a body, the rate of heat generation inside the body, and the rate of heat stored by the body must be balanced

$$\rho c_p \frac{\partial u}{\partial t} + \nabla^T \mathbf{q} = Q \quad (2.1)$$

where  $\mathbf{q}$  is the heat flux vector defined as  $[q_x, q_y, q_z]^T$ ,  $\nabla$  is the gradient operator defined for a rectangular coordinate system as  $[\frac{\partial}{\partial x}, \frac{\partial}{\partial y}, \frac{\partial}{\partial z}]^T$ , and  $\rho$  and  $c_p$  are the density and the specific heat of the material, respectively [14]. The internal heat generation,  $Q$ , is a scalar function of position and is associated with conversion of some other form of energy, such as chemical, electrical, or nuclear, to thermal energy. The heat flux is related to the temperature gradient by Fourier's Law

$$\mathbf{q} = -\boldsymbol{\kappa} \nabla u \quad (2.2)$$

where  $\boldsymbol{\kappa}$  is the thermal conductivity tensor, which is defined for an anisotropic material as the following matrix of thermal conductivities

$$\boldsymbol{\kappa} = \begin{bmatrix} k_{xx} & k_{xy} & k_{xz} \\ k_{yx} & k_{yy} & k_{yz} \\ k_{zx} & k_{zy} & k_{zz} \end{bmatrix} \quad (2.3)$$

Since heat flows in the direction of decreasing temperature, and the gradient points in the opposite direction, the minus sign is included in (2.2) to make the heat flow a positive quantity. Substitution of (2.2) into (2.1) results in the partial differential equation for temperature

$$\rho c_p \frac{\partial u}{\partial t} - \nabla^T (\boldsymbol{\kappa} \nabla u) = Q \quad (2.4)$$

To allow for comparison with exact solutions, the steady state heat conduction in a simple two-dimensional domain made of an orthotropic material will be considered in this research. The simplification to two dimensions from three dimensions is made by assuming the domain is infinitely long in the  $y$ -direction. The domain,  $\Omega = (0, L) \times \left(-\frac{d}{2}, \frac{d}{2}\right)$ , is shown in Figure 2.1, and has length  $L$  and thickness  $d$  with the boundary denoted by  $\partial\Omega$ . The thermal conductivity of a two-dimensional orthotropic

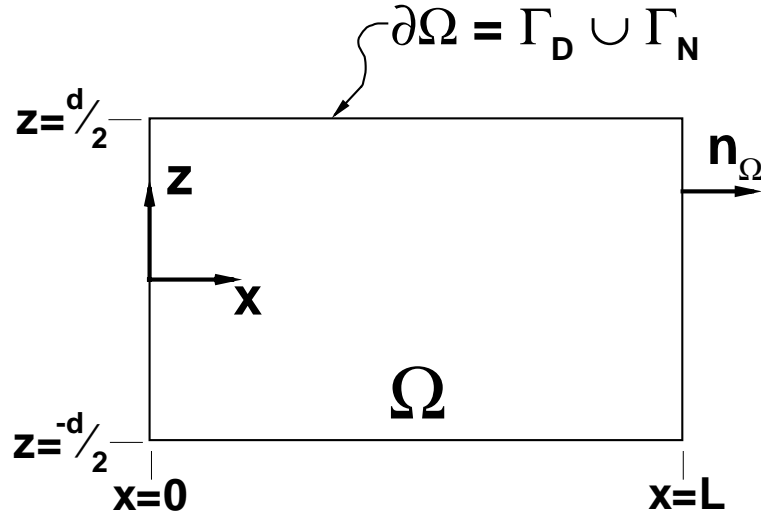


Figure 2.1: Two-dimensional domain  $\Omega$  for an orthotropic material.

material is different in the two principle directions, in this case the  $x$  and  $z$  directions, and is assumed to be constant.

$$\boldsymbol{\kappa} = \begin{bmatrix} k_x & 0 \\ 0 & k_z \end{bmatrix} \quad (2.5)$$

For steady-state conditions, (2.4) becomes a second-order elliptic partial differential equation. For this research, the boundary conditions are defined on each edge as either

a Dirichlet or a Neumann boundary condition. A Dirichlet boundary, denoted by  $\Gamma_D$ , is defined as a boundary on which the temperature is specified and is also called an essential boundary condition. A Neumann boundary, denoted by  $\Gamma_N$ , is defined as a boundary on which the heat flux is specified and is also called a natural boundary condition. The outward unit normal to the boundary is denoted by  $\mathbf{n}_\Omega = [n_x, 0, n_z]^T$ . The boundary value problem for the temperature,  $u(x, z)$ , in the domain is given by

$$\begin{aligned} -\nabla^T (\boldsymbol{\kappa} \nabla u) &= Q \quad \text{in } \Omega \\ -(\boldsymbol{\kappa} \nabla u)^T \mathbf{n}_\Omega &= q_s \quad \text{on } \Gamma_N \\ u &= u_s \quad \text{on } \Gamma_D \end{aligned} \tag{2.6}$$

where  $q_s$  and  $u_s$  are not necessarily constant.

## 2.2 Weak Formulation

The finite element method is based on the weak form, or the variational form, of the boundary value problem (2.6). A weak form is a weighted-integral statement of a differential equation in which the differentiation is distributed among the dependent variable and a weight function and includes the natural boundary conditions of the problem [15]. To obtain the weak form of the boundary value problem for heat conduction, (2.6) is multiplied by a scalar test function  $v$  and integrated by parts

$$\int_{\Omega} -\nabla^T (\boldsymbol{\kappa} \nabla u) v \, d\Omega = \int_{\Omega} Q v \, d\Omega \tag{2.7}$$

$$-(\boldsymbol{\kappa} \nabla u)^T \mathbf{n}_\Omega v \Big|_{\partial\Omega} + \int_{\Omega} (\boldsymbol{\kappa} \nabla u)^T \nabla v \, d\Omega = \int_{\Omega} Q v \, d\Omega \tag{2.8}$$

$$-(\boldsymbol{\kappa} \nabla u)^T \mathbf{n}_\Omega v \Big|_{\Gamma_D} - (\boldsymbol{\kappa} \nabla u)^T \mathbf{n}_\Omega v \Big|_{\Gamma_N} + \int_{\Omega} (\boldsymbol{\kappa} \nabla u)^T \nabla v \, d\Omega = \int_{\Omega} Q v \, d\Omega \tag{2.9}$$

The test function is required to be zero on  $\Gamma_D$ , which simplifies (2.9) to a general problem statement for the temperature in the domain where the boundary conditions in (2.6) have been applied. Find the temperature  $u = u(x, z)$  such that  $u = u_s$  on  $\Gamma_D$

and

$$\int_{\Omega} (\boldsymbol{\kappa} \nabla u)^T \nabla v \, d\Omega = \int_{\Omega} Qv \, d\Omega - \int_{\Gamma_N} q_s v \, ds \quad (2.10)$$

for all admissible test functions  $v$  where  $s$  denotes a boundary. If  $B(u, v)$  and  $L(v)$  are defined as

$$\begin{aligned} B(u, v) &= \int_{\Omega} (\boldsymbol{\kappa} \nabla u)^T \nabla v \, d\Omega \\ L(v) &= \int_{\Omega} Qv \, d\Omega - \int_{\Gamma_N} q_s v \, ds \end{aligned} \quad (2.11)$$

then the problem statement can be expressed in abstract form. Find  $u \in V(\Omega)$  such that  $u = u_s$  on  $\Gamma_D$  and

$$B(u, v) = L(v) \quad \text{for all admissible } v \in V(\Omega) \quad (2.12)$$

where  $V(\Omega)$  is defined as a subspace of  $H^1(\Omega)$ , the Hilbert space consisting of functions with square integrable first derivatives [16].

## 2.3 Finite Element Method

The solution to (2.12) is also the solution to (2.6) and is not an approximation. But since the solution space  $V(\Omega)$  is infinite-dimensional, it is difficult to solve for the exact solution. The finite element method is used to construct a finite-dimensional subspace of  $V(\Omega)$ , denoted by  $\hat{V}(\Omega)$ , by subdividing the domain into a collection of elements and selecting a set of basis functions. The abstract form of the finite element method is to find  $\hat{u} \in \hat{V}(\Omega)$  such that  $u = u_s$  on  $\Gamma_D$  and

$$B(\hat{u}, \hat{v}) = L(\hat{v}) \quad (2.13)$$

for all admissible test functions  $\hat{v} \in \hat{V}(\Omega)$ . This allows an approximation to the exact solution to be found, and the larger the choice for the subspace  $\hat{V}(\Omega)$ , the closer to  $V(\Omega)$  it becomes, therefore making the approximation more accurate. The following

sections describe the method used to approximate the solution to (2.12), hierarchical modelling combined with p-version finite elements.

### 2.3.1 Hierarchical Modelling

In this research, hierarchical modelling refers to the process of describing the solution on a domain whose spatial dimension is reduced by one. The geometry of the rectangular domain in Figure 2.1 can be described as a one-dimensional domain, a straight line of length  $L$  with a constant thickness  $d$ . More general geometries can be described in this manner by allowing the thickness to vary along the length. This approach is commonly used in structural mechanics to represent beams, flat plates, and curved shells.

The approach used in structural mechanics to represent the two-dimensional solution on the one-dimensional domain is usually a global approach. The solution is assumed to have a polynomial distribution through the thickness of the domain, and the degree of the polynomial, denoted by  $p_z$ , is assumed to be constant throughout the domain. This assumption transforms a single partial differential equation on the original domain into a system containing  $p_z + 1$  differential equations on the dimensionally-reduced domain. The finite element method is then applied to each differential equation in the system. In the hierarchical modelling approach used in this research, the solution is assumed to have a polynomial distribution through the thickness of the domain after the dimensionally-reduced domain has been subdivided into elements. This allows the hierarchical model order,  $p_z$ , to vary along the length of an element, and therefore throughout the domain. Also, the hierarchical model order,  $p_z$ , can be easily increased as part of the finite element method.

For simplicity, the hierarchical modelling approach will be described for a two-node linear finite element. The extension to higher-order (p-version) finite elements

will be described in the next section. The one-dimensional domain representing the rectangular plate is divided into  $N$  elements as shown in Figure 2.2. As with tradi-

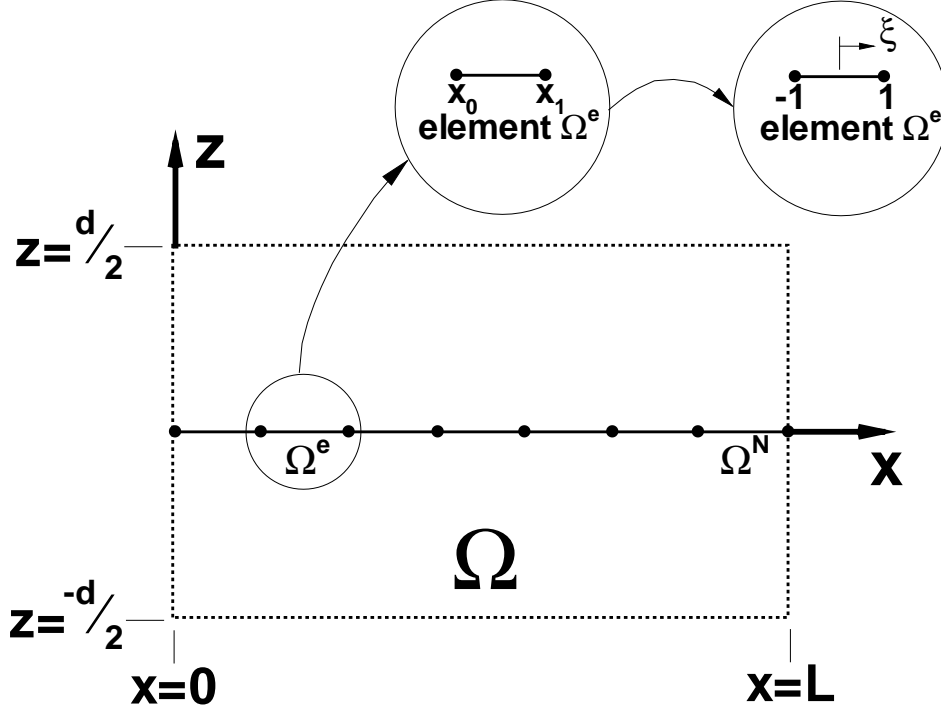


Figure 2.2: Discretization of the domain for the finite element method.

tional finite element methods for one-dimensional problems, the solution on a typical element,  $\Omega^e$ , is assumed to vary linearly along the length of the element, and is written in terms of a local coordinate system

$$\hat{u}|_{\Omega^e} = \frac{1}{2}(1 - \xi)u_0 + \frac{1}{2}(1 + \xi)u_1 \quad (2.14)$$

The mapping for each element in the global domain from  $(x_0, x_1)$  to the local domain  $(-1, 1)$  is given by

$$\xi = \frac{2(x - x_0)}{x_1 - x_0} - 1 \quad (2.15)$$

However for hierarchical modelling, the nodal unknowns  $u_0$  and  $u_1$  are not constants, they are functions of the through-thickness direction

$$\hat{u}|_{\Omega^e} = \frac{1}{2}(1 - \xi)u_0(z) + \frac{1}{2}(1 + \xi)u_1(z) \quad (2.16)$$

where the subscripts 0 and 1 denote the left and right nodes of the element respectively. The unknown functions  $u_0(z)$  and  $u_1(z)$  are assumed to be polynomials of degree  $p_{z0}$  and  $p_{z1}$

$$\begin{aligned} u_0 &= \sum_{i=0}^{p_{z0}} \psi_i(\eta) u_{0i} \\ u_1 &= \sum_{i=0}^{p_{z1}} \psi_i(\eta) u_{1i} \end{aligned} \quad (2.17)$$

where  $p_{z0}$  and  $p_{z1}$  are positive integers,  $\eta = \frac{2z}{d}$  is a normalized through-thickness coordinate,  $\psi_i$  are polynomial basis functions, and  $u_{ji}$  are the unknown constants, also called the element degrees of freedom. The complete expression for the approximate solution on an element is obtained by substituting (2.17) into (2.16) to get

$$\hat{u}|_{\Omega^e} = \frac{1}{2}(1 - \xi) \sum_{i=0}^{p_{z0}} \psi_i(\eta) u_{0i} + \frac{1}{2}(1 + \xi) \sum_{i=0}^{p_{z1}} \psi_i(\eta) u_{1i} \quad (2.18)$$

The basis functions for the through-thickness polynomial approximations are the integrated Legendre polynomials, which are shown to be well suited for computer implementation and have favorable properties for numerical stability by Babuska et. al in [4] and are given by

$$\begin{aligned} \psi_0 &= 1 \\ \psi_1 &= \eta \\ \psi_i &= \sqrt{\frac{2i-1}{2}} \int_{-1}^{\eta} P_{i-1}(\xi) d\xi \\ &= \frac{1}{\sqrt{2(2i-1)}} (P_i(\eta) - P_{i-2}(\eta)), \quad i = 2, 3, \dots, p_z + 1 \end{aligned} \quad (2.19)$$

where  $P_i$  is the Legendre polynomial of the first kind of order  $i$  given by [17]

$$\begin{aligned} P_0(\eta) &= 1 \\ P_1(\eta) &= \eta \\ P_i(\eta) &= \frac{1}{i} [(2i-1)\eta P_{i-1}(\eta) - (i-1)P_{i-2}(\eta)] \quad i = 2, 3, \dots \end{aligned} \quad (2.20)$$

The integration in (2.19) is accomplished by applying the properties of Legendre polynomials. Note that the usual linear approximation for a one-dimensional element is a special case of the hierarchical model, obtained when  $p_{z0} = p_{z1} = 0$  in (2.18). When the degree of the through-thickness polynomial does not vary along the element length, that is when  $p_{z0} = p_{z1} = p_z$ , (2.18) can be written as

$$\begin{aligned}\hat{u}|_{\Omega^e} &= \sum_{i=0}^{p_z} \left[ \frac{1}{2}(1 - \xi)u_{0i} + \frac{1}{2}(1 + \xi)u_{1i} \right] \psi_i(\eta) \\ &= \sum_{j=0}^1 \sum_{i=0}^{p_z} \phi_j(\xi) \psi_i(\eta) u_{ji}\end{aligned}\tag{2.21}$$

### 2.3.2 P-Element Approximation

The traditional approach to higher-order one-dimensional finite elements requires that an element with a polynomial approximation of degree  $p_x$  contain  $p_x + 1$  evenly-spaced nodes. The basis functions for such an element are the Lagrange polynomials, and the element is referred to as a Lagrange element. A Lagrange polynomial basis function is associated with each node of the element along with a corresponding degree of freedom which is the value of the unknown at that point. Quadratic and cubic Lagrange elements and the corresponding basis functions are shown in Figure 2.3.

The p-version approach to higher-order, one-dimensional, finite elements is to add a single node in the middle of the element, and a set of higher-order polynomials that are zero at the endpoints are added to the usual linear basis functions associated with the end nodes. The number of basis functions, and hence the number of unknown coefficients, associated with the middle node is determined by the degree of the polynomial approximation  $p_x$ . Specifically, there are  $p_x - 1$  basis functions associated with the middle node. Elements of this type are often referred to as hierarchical p-elements, because increasing the order of the elements is accomplished by simply adding a basis function to the existing set, as indicated in Figure 2.4, without

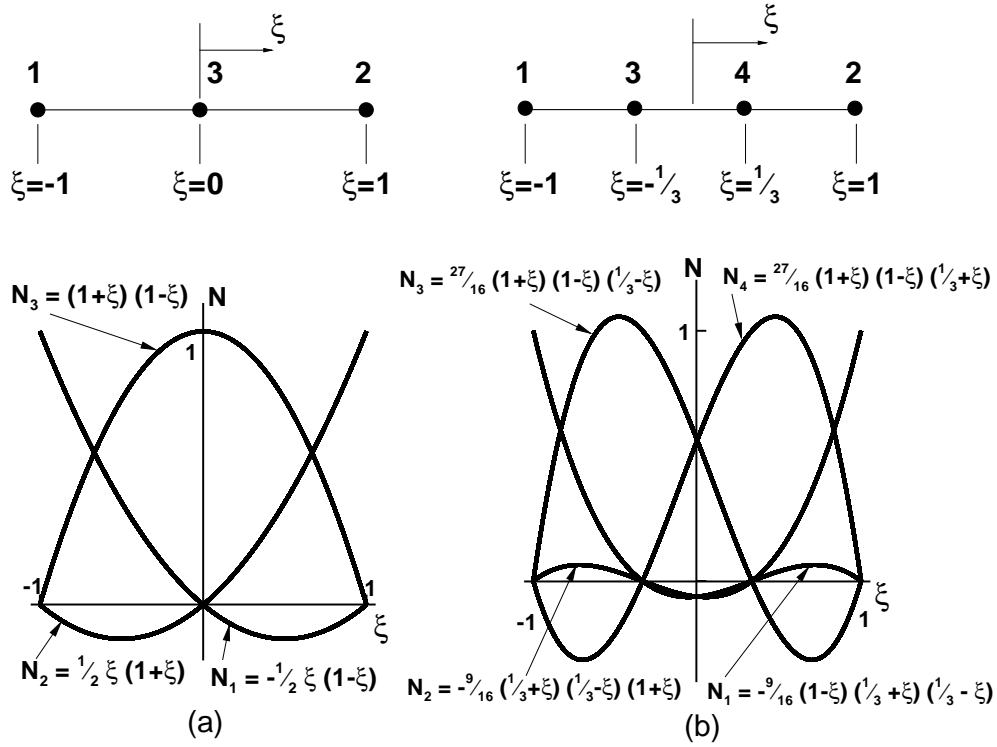


Figure 2.3: One-dimensional (a) quadratic Lagrange element and (b) cubic Lagrange element with corresponding basis functions.

the requirement of mesh regeneration. The finite element approximation in a typical element is written

$$\hat{u}|_{\Omega^e} = \frac{1}{2}(1 - \xi)u_0 + \frac{1}{2}(1 + \xi)u_1 + \sum_{i=2}^{p_x} \phi_i(\xi)a_i = \sum_{i=0}^{p_x} \phi_i(\xi)a_i \quad (2.22)$$

The degrees of freedom corresponding to the middle node do not represent the value of the solution at the midpoint and are therefore denoted by the symbol  $a_i$ . The unknowns  $u_0$  and  $u_1$  are combined into the set of unknowns,  $a_i$ . In other words,  $a_0 = u_0$  and  $a_1 = u_1$ . The basis functions used for the one-dimensional element, i.e., for the polynomial approximation in the  $x$ -direction, are similar to the through-thickness basis functions and are given by

$$\begin{aligned} \phi_0 &= \frac{1}{2}(1 - \xi) \\ \phi_1 &= \frac{1}{2}(1 + \xi) \end{aligned}$$

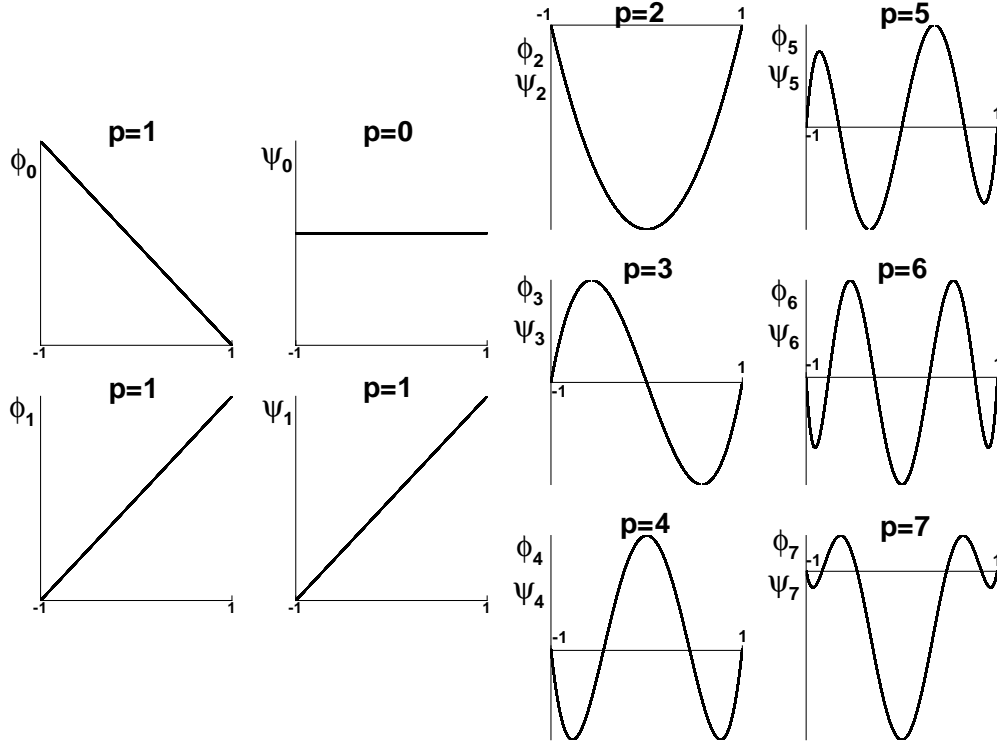


Figure 2.4: Element basis functions,  $\phi$  and  $\psi$ , for  $p = 1$  through 7.

$$\begin{aligned}
\phi_i &= \sqrt{\frac{2i-1}{2}} \int_{-1}^{\xi} P_{i-1}(\xi) d\xi \\
&= \frac{1}{\sqrt{2(2i-1)}} (P_i(\xi) - P_{i-2}(\xi)), \quad i = 2, 3, \dots, p_x + 1
\end{aligned} \tag{2.23}$$

The procedure for combining hierarchical modelling with p-version elements is the same as described in the previous section. The constant unknowns in (2.22) are replaced by polynomial functions in the through-thickness direction

$$\hat{u}|_{\Omega^e} = \frac{1}{2}(1-\xi)u_0(z) + \frac{1}{2}(1+\xi)u_1(z) + \sum_{i=2}^{p_x} \phi_i(\xi)a_i(z) = \sum_{i=0}^{p_x} \phi_i(\xi)a_i(z) \tag{2.24}$$

where

$$\begin{aligned}
u_0 &= \sum_{i=0}^{p_{z0}} \psi_i(\eta)u_{0i} \\
u_1 &= \sum_{i=0}^{p_{z1}} \psi_i(\eta)u_{1i} \\
a_j &= \sum_{i=0}^{p_{z2}} \psi_i(\eta)a_{ij}
\end{aligned} \tag{2.25}$$

Again, if the hierarchical model order is constant for the element,  $p_{z0} = p_{z1} = p_{z2} = p_z$ , then the approximate solution in an element can be written

$$\begin{aligned}\hat{u}|_{\Omega^e} &= \sum_{i=0}^{p_z} \left[ \frac{1}{2}(1-\xi)u_{0i} + \frac{1}{2}(1+\xi)u_{1i} + \sum_{j=2}^{p_x} \phi_j(\xi)a_{ji} \right] \psi_i(\eta) \\ \hat{u}|_{\Omega^e} &= \sum_{j=0}^{p_x} \sum_{i=0}^{p_z} \phi_j(\xi)\psi_i(\eta)a_{ji}\end{aligned}\quad (2.26)$$

The finite element approximation for the temperature distribution in an element is determined by the unknown coefficients,  $a_{ji}$ . The basis functions,  $\phi_j(\xi)$  and  $\psi_i(\eta)$  are polynomials of degree  $p_x$  and  $p_z$ , respectively. The number of unknown coefficients for the element is determined by  $(p_x + 1) \times (p_z + 1)$ .

### 2.3.3 Element Matrices

The weak form of the boundary value problem, (2.13), is an integral equation over the entire domain, which can be represented by a sum of integrals over each element in the domain. The domain of an element, denoted by  $\Omega^e$ , is defined as  $(x_0, x_1) \times (\frac{-d}{2}, \frac{d}{2})$ , where  $x_0$  and  $x_1$  are the x-coordinates of the end nodes. The local contributions from the elements are combined into a global problem to allow for the solution to the finite element approximation. Note that an element end node is shared by a neighboring element. Since the unknown coefficients are associated with a node, the approximate temperature solution is continuous across element interfaces. Equation (2.13) is written as a sum of element contributions

$$\sum_{e=1}^{N_{el}} \int_{\Omega^e} (\boldsymbol{\kappa} \nabla \hat{u})^T \nabla \hat{v} \, d\Omega^e = \sum_{e=1}^{N_{el}} \int_{\Omega^e} Q \hat{v} \, d\Omega^e - \int_{\partial\Omega^e \cap \Gamma_N} q_s \hat{v} \, ds \quad (2.27)$$

provided that

$$\sum_{e=1}^{N_{el}} \Omega^e = \Omega \quad (2.28)$$

$$\sum_{e=1}^{N_{el}} \partial\Omega^e \cap \Gamma_N = \Gamma_N \quad (2.29)$$

Here  $N_{el}$  denotes the total number of elements in the mesh and  $\partial\Omega^e \cap \Gamma_N$  denotes the part of the boundary of an element which lies on  $\Gamma_N$ . To simplify the derivation of the finite element matrices the approximate solution in (2.26) can be written in compact notation using outer tensor products

$$\hat{u}|_{\Omega^e} = \sum_{i=0}^{p_x} \sum_{j=0}^{p_z} \phi_i(\xi) \psi_j(\eta) a_{ij} = (\boldsymbol{\phi} \otimes \boldsymbol{\psi})^T \mathbf{a}_e = \boldsymbol{\chi}^T \mathbf{a}_e \quad (2.30)$$

The symbol  $\otimes$  represents the outer tensor product, and  $\boldsymbol{\phi}$  is a vector of length  $(p_x + 1)$ ,  $\boldsymbol{\psi}$  is a vector of length  $(p_z + 1)$ , and  $\boldsymbol{\chi}$  and  $\mathbf{a}_e$  are vectors of length  $(p_x + 1) \times (p_z + 1)$ .

The outer tensor product [17] of an  $n \times n$  matrix  $\mathbf{A}$  with an  $m \times m$  matrix  $\mathbf{B}$  is given by

$$\begin{bmatrix} A_{11} & A_{12} & \cdots & A_{1n} \\ A_{21} & A_{22} & \cdots & A_{2n} \\ \vdots & \vdots & \cdots & \vdots \\ A_{n1} & A_{n2} & \cdots & A_{nn} \end{bmatrix} \otimes \begin{bmatrix} B_{11} & \cdots & B_{1m} \\ \vdots & \cdots & \vdots \\ B_{m1} & \cdots & B_{mm} \end{bmatrix} = \begin{bmatrix} A_{11}\mathbf{B} & A_{12}\mathbf{B} & \cdots & A_{1n}\mathbf{B} \\ A_{21}\mathbf{B} & A_{22}\mathbf{B} & \cdots & A_{2n}\mathbf{B} \\ \vdots & \vdots & \cdots & \vdots \\ A_{n1}\mathbf{B} & A_{n2}\mathbf{B} & \cdots & A_{nn}\mathbf{B} \end{bmatrix} \quad (2.31)$$

There are a variety of choices for the test function,  $\hat{v}$ , which results in a system of equations from (2.27). The Bubnov-Galerkin method, commonly referred to simply as the Galerkin method, defines the test function to be the same as the functions used in the approximation of the solution,  $\hat{u}$ , and will be used in this paper [18]. Substituting the approximate solution (2.30) for  $\hat{u}$  and  $\chi_i$ ,  $i = 1, \dots, (p_x + 1) \times (p_z + 1)$  for  $\hat{v}$ , into (2.27) results in the system of equations

$$\sum_{e=1}^{N_{el}} \left[ \int_{\Omega^e} \nabla \boldsymbol{\chi} (\boldsymbol{\kappa} \nabla \boldsymbol{\chi})^T d\Omega^e \mathbf{a}_e \right] = \sum_{e=1}^{N_{el}} \left[ \int_{\Omega^e} Q \boldsymbol{\chi} d\Omega^e - \int_{\Gamma_N^e} q_s \boldsymbol{\chi} ds \right] \quad (2.32)$$

Here the gradient of the vector  $\boldsymbol{\chi}$  is defined as the gradient operating on each element of the vector. This equation can be written in matrix form as

$$\sum_{e=1}^{N_{el}} (\mathbf{A}_{\Omega^e} \mathbf{a}_e) = \sum_{e=1}^{N_{el}} \mathbf{F}_{\Omega^e} \quad (2.33)$$

The element matrix  $\mathbf{A}_{\Omega^e}$  is defined in terms of a local mass and stiffness matrix using the outer tensor product as

$$\begin{aligned}
\mathbf{A}_{\Omega^e} &= \int_{\Omega^e} \nabla \boldsymbol{\chi} (\boldsymbol{\kappa} \nabla \boldsymbol{\chi})^T d\Omega^e \\
&= \int_{\Omega^e} \left[ k_x \frac{\partial \boldsymbol{\chi}}{\partial x} \frac{\partial \boldsymbol{\chi}^T}{\partial x} + k_z \frac{\partial \boldsymbol{\chi}}{\partial z} \frac{\partial \boldsymbol{\chi}^T}{\partial z} \right] d\Omega^e \\
&= k_x \int_{x_0}^{x_1} \frac{\partial \boldsymbol{\phi}}{\partial x} \frac{\partial \boldsymbol{\phi}^T}{\partial x} dx \otimes \int_{-\frac{d}{2}}^{\frac{d}{2}} \boldsymbol{\psi} \boldsymbol{\psi}^T dz + \\
&\quad k_z \int_{x_0}^{x_1} \boldsymbol{\phi} \boldsymbol{\phi}^T dx \otimes \int_{-\frac{d}{2}}^{\frac{d}{2}} \frac{\partial \boldsymbol{\psi}}{\partial z} \frac{\partial \boldsymbol{\psi}^T}{\partial z} dz \\
&= k_x \mathbf{K}_x \otimes \mathbf{M}_z + k_z \mathbf{M}_x \otimes \mathbf{K}_z
\end{aligned} \tag{2.34}$$

where  $\mathbf{M}$  denotes a local mass matrix and  $\mathbf{K}$  denotes a local stiffness matrix. The element load vector,  $\mathbf{F}_{\Omega^e}$ , is defined as

$$\mathbf{F}_{\Omega^e} = \int_{\Omega^e} Q \boldsymbol{\chi} d\Omega^e - \int_{\Gamma_N^e} q_s \boldsymbol{\chi} ds \tag{2.35}$$

### 2.3.4 Global System of Equations

The global system equations, (2.33), are written

$$\mathbf{A} \mathbf{a} = \mathbf{F} \tag{2.36}$$

where  $\mathbf{A}$  and  $\mathbf{F}$  are the global matrices formed by assembling each  $\mathbf{A}_{\Omega^e}$  and  $\mathbf{F}_{\Omega^e}$ , respectively, and  $\mathbf{a}$  is the global vector of unknowns. The element vector of unknowns,  $\mathbf{a}_e$ , in (2.30), (2.32), and (2.33) is an element ordering of  $\mathbf{a}$  with entries only for the unknowns associated with the nodes of the elements. The process of assembly is rather straightforward and can be found in any finite element textbook, such as [15], [19], and [20]. The approximate solution,  $\hat{u}$ , is determined by applying boundary conditions to the global system of equations and solving the matrix equation for the unknowns  $\mathbf{a}$ .

The Dirichlet boundary conditions in (2.10) are enforced on the system of equations using the penalty method [19]. Recall the form of  $\hat{u}$  from (2.26)

$$\hat{u}|_{\Omega^e} = \sum_{i=0}^{p_z} \left[ \frac{1}{2}(1-\xi)u_{0i} + \frac{1}{2}(1+\xi)u_{1i} + \sum_{j=2}^{p_x} \phi_j(\xi)a_{ji} \right] \psi_i(\eta) \quad (2.37)$$

If the specified temperature is on the left side of an element, at  $\xi = -1$ , then  $\phi_j(\xi)$  is zero for  $j = 2, \dots, p_x$  and  $\hat{u}$  becomes

$$\hat{u}|_{\Omega^e} (\xi = -1) = \sum_{i=0}^{p_z} \psi_i(\eta)u_{0i} \quad (2.38)$$

The value of  $\hat{u}$  at this boundary is specified to be  $u_s$ , therefore

$$(1)u_{00} + \sum_{i=1}^{p_z} \psi_i(\eta)u_{0i} = u_s \quad (2.39)$$

To enforce this boundary condition, we set  $u_{00} = u_s$  and  $u_{0i} = 0$  for  $i = 1, \dots, p_z$ . If the specified temperature is on the right side of an element, at  $\xi = 1$ , we set  $u_{10} = u_s$  and  $u_{1i} = 0$  for  $i = 1, \dots, p_z$ . Using the penalty method, the local coefficient matrix  $\mathbf{A}_{\Omega^e}$  and the local load vector  $\mathbf{F}_{\Omega^e}$  are modified by using a large number,  $C$ , which is several orders of magnitude larger than the components of  $\mathbf{A}$ . A general rule of thumb for choosing the value of  $C$  is to use  $C = \max|A_{ij}| \times 10^4$ . The constant  $C$  is added to each of the diagonal elements in  $\mathbf{A}_{\Omega^e}$  corresponding to the degrees of freedom on the Dirichlet boundary, and  $C$  is multiplied by the specified temperature on the boundary and added to the corresponding components in the load vector,  $\mathbf{F}_{\Omega^e}$ . For example, to enforce the Dirichlet boundary condition on the left end of an element

$$\begin{aligned} A_{\Omega_{ii}^e} &= A_{\Omega_{ii}^e} + C \quad \text{for } i = 0, \dots, p_z \\ F_{\Omega_i^e} &= F_{\Omega_i^e} + Cu_s \quad \text{for } i = 0 \end{aligned} \quad (2.40)$$

The Neumann boundary conditions, or natural boundary conditions, in (2.6) are included in the right hand side of the weak form (2.10) and are thus included in  $\mathbf{F}_{\Omega^e}$ .

Enforcement of the boundary conditions along  $\Gamma_D$  causes the system of equations to be nonsingular so that a solution to the global system of equations exists.

The numerical accuracy of the solution of the global system of equations depends on the conditioning of the  $\mathbf{A}$  matrix and the choice of the value of  $C$ . The condition number of a matrix is defined as the ratio of the largest eigenvalue to the smallest eigenvalue. A matrix is singular if its condition number is infinite since at least one eigenvalue is zero, and although the  $\mathbf{A}$  matrix is not singular due to the enforcement of the Dirichlet boundary conditions, a large condition number limits the accuracy to which a solution can be obtained. If the value of  $C$  in the penalty approach is chosen to be large enough, then  $u \approx u_s$  on  $\Gamma_D$ . Generally this boundary condition is satisfied to machine numerical precision with the proper choice for  $C$  and a low condition number. Gauss elimination can be used to solve the system of equations which involves row reduction to obtain an upper triangular matrix. The system matrices are sparse, having a relatively small number of nonzero entries, due to the choice of the basis functions. The derivatives of the basis functions are orthogonal to each other except for the nodal basis functions, denoted with the 0 and 1 subscript in (2.23) and (2.19). The local stiffness matrices, defined as  $\mathbf{K}_x$  and  $\mathbf{K}_z$  in (2.34), use the derivatives of the basis functions, and therefore are almost diagonal. There are off-diagonal nonzero entries in the first and second rows and columns since the nodal basis functions do not have the property of orthogonal derivatives. The zero entries in the stiffness and the small number of zero entries in the local mass matrices create a sparse  $\mathbf{A}_{\Omega^e}$  matrix when the outer tensor product, defined in (2.31), is used.

The relatively small number of nonzero entries makes it inefficient to store the zero entries. To save memory and time, the global system is solved using a sparse gauss matrix solver [21].

# Chapter 3

## A Posteriori Error Estimation

There are essentially two types of error estimates, *a priori* and *a posteriori*. *A priori* estimates are theoretical bounds on the error in an approximate solution, and establish the rate of convergence of the error for a particular method. These bounds are a function of the exact solution and the parameters that influence the accuracy of the approximate solution. For p-version finite element methods, these parameters are the mesh size,  $h$ , and the degree,  $p$ , of the polynomial approximation in an element. *A posteriori* error estimates use the approximate solution itself to estimate its error. They fall into two categories: implicit and explicit. Explicit error estimates are fast and computationally inexpensive as they typically involve post-processing of the finite element solution. Implicit error estimates are obtained by solving an additional boundary value problem for the error with the approximate solution as input data. Implicit error estimates are more expensive than explicit error estimates, but they are also more reliable and more accurate. This research focuses on the element residual error method, which is an implicit type *a posteriori* error estimate. The global residual is defined as

$$R(v) = L(v) - B(\hat{u}, v)$$

It provides information on how close the approximate solution is to satisfying the boundary value problem. This chapter discusses the method and approach to pre-

dicting the global error in the finite element solution to the two-dimensional boundary value problem in (2.12). The global error estimate is a sum of element error estimates obtained by solving an element boundary value problem with the element residual analogous to a heat source term. The element residual error method developed by Ainsworth and Oden [1] for the total error is first described. The performance of the error estimate is then demonstrated on two example problems. When using the hierarchical modelling approach, the mesh size  $h$ , the through-thickness polynomial order  $p_z$ , and the in-plane polynomial order  $p_x$  are parameters that affect the accuracy of the solution. A directional error estimate is proposed to distinguish the modelling error ( $p_z$ ) from the finite element error ( $p_x$  and  $h$ ). Its performance is investigated on two example problems.

### 3.1 Element Residual Method

The error in the finite element solution is the difference between the exact and the finite element solutions,  $e = u - \hat{u}$ . The weak form of the boundary value problem for the error is obtained by subtracting  $B(\hat{u}, v)$  from both sides of (2.12).

$$\begin{aligned}
 B(u, v) - B(\hat{u}, v) &= L(v) - B(\hat{u}, v) \\
 B(e, v) &= L(v) - B(\hat{u}, v) \\
 B(e, v) &= R(v) \quad \forall v \in V(\Omega)
 \end{aligned} \tag{3.1}$$

The solution of this global equation yields the actual error, but the solution space  $V(\Omega)$ , defined as a subspace of  $H^1(\Omega)$ , is of infinite dimension. The finite element approximation described in Chapter 2 for the temperature can also be used to approximate the solution to (3.1) for the error. However, if the subspace used to approximate the error is the same subspace  $\hat{V}(\Omega)$  that was used for the finite element approximation, the result will be that the error is zero. Since the right hand side of (3.1) with

$v \in \hat{V}(\Omega)$  is precisely what was solved for the finite element solution,  $R(v) = 0$  for every  $v \in \hat{V}(\Omega)$ . Therefore to obtain a nontrivial approximation for the error, a larger subspace must be used. A simple approach to constructing a larger subspace is to increase the polynomial degree of the approximation on each element in both the through-thickness and in-plane directions. Solving the global error problem on this enriched polynomial space would, however, require more computation time than originally required to solve the heat conduction problem. A more efficient approach is to solve a local (or element) boundary value problem to provide an estimate of the error on each element. The local boundary value problem for the error in each element is derived from the original differential equation for the temperature. The global differential equation (2.6) holds true for any point in the solution domain. Therefore this differential equation also holds true for any collection of points defining an arbitrary subdomain or element, making (2.6) valid for any element. With the finite element solution,  $\hat{u}$ , in hand, the quantity  $\nabla^T(\boldsymbol{\kappa}\nabla\hat{u})$  is added to both sides of (2.6) defined on each element

$$\begin{aligned}
+\nabla^T(\boldsymbol{\kappa}\nabla\hat{u}) - \nabla^T(\boldsymbol{\kappa}\nabla u) &= Q + \nabla^T(\boldsymbol{\kappa}\nabla\hat{u}) \\
-\nabla^T(\boldsymbol{\kappa}\nabla e) &= Q + \nabla^T(\boldsymbol{\kappa}\nabla\hat{u}) \quad \text{on element } \Omega^e
\end{aligned} \tag{3.2}$$

Appropriate boundary conditions for this equation will be considered with the weak formulation, obtained by multiplying (3.2) by a test function  $v$  and integrating by parts

$$\begin{aligned}
-\int_{\Omega^e} \nabla^T(\boldsymbol{\kappa}\nabla e)v \, d\Omega^e &= \int_{\Omega^e} Qv \, d\Omega^e + \int_{\Omega^e} \nabla^T(\boldsymbol{\kappa}\nabla\hat{u})v \, d\Omega^e \\
-\left[ \int_{\partial\Omega^e} (\boldsymbol{\kappa}\nabla e)^T \mathbf{n}_{\Omega^e} v \, ds - \int_{\Omega^e} (\boldsymbol{\kappa}\nabla e)^T \nabla v \, d\Omega^e \right] &= \int_{\Omega^e} Qv \, d\Omega^e + \int_{\partial\Omega^e} (\boldsymbol{\kappa}\nabla\hat{u})^T \mathbf{n}_{\Omega^e} v \, ds \\
&\quad - \int_{\Omega^e} (\boldsymbol{\kappa}\nabla\hat{u})^T \nabla v \, d\Omega^e
\end{aligned} \tag{3.3}$$

Substituting  $\hat{u} = u - e$  into the boundary integral terms simplifies (3.3) to

$$\begin{aligned} \int_{\Omega^e} (\boldsymbol{\kappa} \nabla e)^T \nabla v \, d\Omega^e &= \int_{\Omega^e} Qv \, d\Omega^e - \int_{\Omega^e} (\boldsymbol{\kappa} \nabla \hat{u})^T \nabla v \, d\Omega^e + \int_{\partial\Omega^e} (\boldsymbol{\kappa} \nabla u)^T \mathbf{n}_{\Omega^e} v \, ds \\ B_{\Omega^e}(e, v) &= F_{\Omega^e}(v) - B_{\Omega^e}(\hat{u}, v) + \int_{\partial\Omega^e} (\boldsymbol{\kappa} \nabla u)^T \mathbf{n}_{\Omega^e} v \, ds \end{aligned} \quad (3.4)$$

where  $F_{\Omega^e}(v)$  is the linear function associated with the source term defined as  $\int_{\Omega^e} Qv \, d\Omega^e$ .

The subscript  $\Omega^e$  on  $B_{\Omega^e}$  and  $F_{\Omega^e}$  denotes a local domain. Equation (3.4) is the weak form of the local error problem. This equation is the element contribution to the global error problem in (3.1), since the exact boundary flux terms in (3.4) sum to zero along interior element boundaries. The actual error satisfies (3.4), but the exact flux in the last term,  $(\boldsymbol{\kappa} \nabla u)^T \mathbf{n}_{\Omega^e}$ , is not known. Therefore an approximation must be made for the flux boundary conditions on each element:

$$\hat{q}_{\Omega^e} \approx -(\boldsymbol{\kappa} \nabla u)^T \mathbf{n}_{\Omega^e} \quad (3.5)$$

Using this approximation for the exact boundary flux in (3.4) results in the local problem to be solved in each element. Find  $e \in V(\Omega^e)$  such that

$$B_{\Omega^e}(e, v) = F_{\Omega^e}(v) - B_{\Omega^e}(\hat{u}, v) - \int_{\partial\Omega^e} \hat{q}_{\Omega^e} v \, ds \quad (3.6)$$

for all admissible  $v \in V(\Omega^e)$ . The next section discusses two approaches to constructing an approximate boundary flux,  $\hat{q}_{\Omega^e}$ , using the finite element solution.

## 3.2 Element Boundary Conditions

The boundary flux  $(\boldsymbol{\kappa} \nabla u)^T \mathbf{n}_{\Omega^e}$  must be determined for each type of element boundary. Three possible types of element boundaries are considered: Dirichlet boundary, Neumann boundary, or interior element boundary. The boundary conditions for the edge of an element that is coincident with a global boundary is straightforward. For an element boundary that is coincident with  $\Gamma_D$ , where the temperature is specified

as a constant, the finite element solution satisfies the essential boundary condition exactly

$$\begin{aligned} u &= \hat{u} = u_s && \text{on } \partial\Omega^e \cap \Gamma_D \\ e &= u - \hat{u} = 0 && \text{on } \partial\Omega^e \cap \Gamma_D \end{aligned} \quad (3.7)$$

and the test function in (3.6) is required to be zero on  $\partial\Omega^e \cap \Gamma_D$ . For an element boundary that is coincident with  $\Gamma_N$ , the applied heat flux is specified in the problem statement as  $q_s$ . For this natural boundary condition,

$$-(\boldsymbol{\kappa} \nabla u)^T \mathbf{n}_{\Omega^e} = q_s \quad \text{on } \partial\Omega^e \cap \Gamma_N \quad (3.8)$$

The third type of boundary that must be considered is the interior element boundary (the interface between two neighboring elements) where an approximation to the exact flux must be made. The choice of the approximate boundary flux determines the accuracy of the error estimate. The next sections discuss two methods of approximating the exact flux on the interior element boundaries, the average flux method and the equilibrated flux method.

### 3.2.1 Average Element Boundary Flux

The finite element approximation results in a flux that is discontinuous across interior element boundaries. One approach to approximating the exact flux on an interior element boundary is to average the fluxes computed from the finite element approximation on the boundary between neighboring elements. Let  $\Omega^{e'}$  denote the neighbor to element  $\Omega^e$  and let  $\gamma$  denote the shared edge, then the average flux on the shared edge is given by

$$\hat{q}_{\Omega^e}|_{\gamma} = \frac{1}{2} \left( -\boldsymbol{\kappa} \nabla \hat{u}_{\Omega^e}|_{\gamma} - \boldsymbol{\kappa} \nabla \hat{u}_{\Omega^{e'}}|_{\gamma} \right)^T \mathbf{n}_{\Omega^e} \quad (3.9)$$

where  $\mathbf{n}_{\Omega^e}$  is the outward unit normal vector to the edge of element  $\Omega^e$ . The average flux, applied to the shared boundary of the neighboring elements, satisfies the

continuity condition

$$\hat{q}_{\Omega^e}|_{\gamma} + \hat{q}_{\Omega^{e'}}|_{\gamma} = 0 \quad \text{on the shared edge } \gamma = \partial\Omega^e \cap \partial\Omega^{e'} \quad (3.10)$$

since  $\mathbf{n}_{\Omega^e} = -\mathbf{n}_{\Omega^{e'}}$  and

$$\begin{aligned} \hat{q}_{\Omega^{e'}}|_{\gamma} &= \frac{1}{2} \left( -\boldsymbol{\kappa} \nabla \hat{u}_{\Omega^{e'}}|_{\gamma} - \boldsymbol{\kappa} \nabla \hat{u}_{\Omega^e}|_{\gamma} \right)^T \mathbf{n}_{\Omega^{e'}} \\ &= -\frac{1}{2} \left( -\boldsymbol{\kappa} \nabla \hat{u}_{\Omega^{e'}}|_{\gamma} - \boldsymbol{\kappa} \nabla \hat{u}_{\Omega^e}|_{\gamma} \right)^T \mathbf{n}_{\Omega^e} \\ &= -\hat{q}_{\Omega^e}|_{\gamma} \end{aligned} \quad (3.11)$$

### 3.2.2 Equilibrated Flux

Another method for approximating the fluxes on the interior element boundary is to develop boundary fluxes that, in addition to satisfying continuity (3.10), satisfy an equilibrium condition for that element [1]. The equilibrated flux method as described in [1] is applicable to general two-dimensional meshes of quadrilateral and triangular p-elements. It simplifies considerably for hierarchical modelling.

The equilibrium condition for an element is derived by integrating (2.6) over an element

$$\begin{aligned} \int_{\Omega^e} -\nabla^T (\boldsymbol{\kappa} \nabla u) \, d\Omega^e &= \int_{\Omega^e} Q \, d\Omega^e \\ \int_{\partial\Omega^e} -(\boldsymbol{\kappa} \nabla u)^T \mathbf{n}_{\Omega^e} \, ds &= \int_{\Omega^e} Q \, d\Omega^e \end{aligned} \quad (3.12)$$

In the second step, integration by parts is used on the left hand side. For steady state conditions, the flux around the boundary of an element must be in equilibrium with the internal heat source. Therefore, the approximate flux must be constructed such that for every element in the mesh

$$\int_{\partial\Omega^e} \hat{q}_{\Omega^e} \, ds = \int_{\Omega^e} Q \, d\Omega^e \quad (3.13)$$

Note that (3.13) is equivalent to setting  $v = 1$  in (3.6), that is,

$$0 = F_{\Omega^e}(1) - B_{\Omega^e}(\hat{u}, 1) - \int_{\partial\Omega^e} \hat{q}_{\Omega^e} \, ds \quad (3.14)$$

since  $B_{\Omega^e}(e, 1)$  and  $B_{\Omega^e}(\hat{u}, 1)$  are zero. The term  $B_{\Omega^e}(\hat{u}, 1)$  is retained in (3.14) because it is part of the element residual and plays an important role in constructing the equilibrated approximate flux. The equilibrium condition (3.14) can be extended to higher orders by replacing 1 in (3.14) with a set of two-dimensional nodal basis functions,  $\theta_n$ , defined at each node  $n$ .

$$F_{\Omega^e}(\theta_n) - B_{\Omega^e}(\hat{u}, \theta_n) - \int_{\partial\Omega^e} \hat{q}_{\Omega^e} \theta_n ds = 0 \quad \text{for } n = 1, \dots, n_\gamma \quad (3.15)$$

The  $\theta_n$ 's represent basis functions associated with the nodes on the boundary of an element. The specific form and the required number,  $n_\gamma$ , of the nodal basis functions along an edge, to be discussed later, will depend on the approximation selected for  $\hat{q}_{\Omega^e}$ .

The approximate flux must satisfy the equilibrium condition (3.15) along with the continuity requirement (3.10) and the Neumann boundary condition (3.8). For hierarchical modelling of a two-dimensional problem, there are only one-dimensional elements in the  $x$ -direction. In order to apply the equilibrated flux method to the hierarchical model, an element is conceptually expanded in the through-thickness direction into a rectangular element. The node and edge numbers are defined on the expanded local element as shown in Figure 3.1. For this expanded element, the top and bottom boundaries of each element are coincident with the global domain boundary,  $\Gamma$ , and therefore an approximate flux is only required for the left and right boundaries, denoted by  $\gamma_2$  and  $\gamma_4$  in Figure 3.1.

The approximation for the left and right element boundary flux is assumed to be a polynomial of degree  $p_z$ , the same as the polynomial degree of the hierarchical model. The approximate flux on an edge,  $\gamma$ , of the boundary of element  $\Omega^e$  is written in terms of the nodal basis functions,  $\boldsymbol{\theta}$ , as

$$\hat{q}_{\Omega^e}|_\gamma = \sum_{i=1}^{p_z+1} \alpha_i \theta_i|_\gamma \quad (3.16)$$

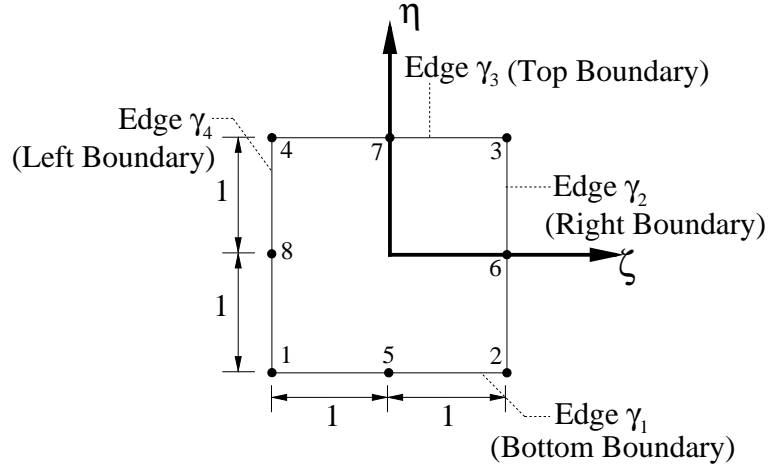


Figure 3.1: Convention for node and edge labels for an expanded local element.

where  $i$  represents the degrees of freedom on the edge  $\gamma$  and  $\alpha_i$  are unknown coefficients. Due to this choice for the approximate boundary flux, the number of nodal basis functions required for the left edge or the right edge is  $n_\gamma = p_z + 1$ . The complete set of two-dimensional basis functions,  $\boldsymbol{\theta}$ , is given by

$$\boldsymbol{\theta} = \left[ \begin{array}{l} \phi_0(\xi)\phi_0(\eta) \\ \phi_1(\xi)\phi_0(\eta) \\ \phi_1(\xi)\phi_1(\eta) \\ \phi_0(\xi)\phi_1(\eta) \\ \phi_2(\xi)\phi_0(\eta) \\ \phi_3(\xi)\phi_0(\eta) \\ \vdots \\ \phi_{p_x}(\xi)\phi_0(\eta) \\ \phi_1(\xi)\phi_2(\eta) \\ \phi_1(\xi)\phi_3(\eta) \\ \vdots \\ \phi_1(\xi)\phi_{p_z}(\eta) \\ \phi_2(\xi)\phi_1(\eta) \\ \phi_3(\xi)\phi_1(\eta) \\ \vdots \\ \phi_{p_x}(\xi)\phi_1(\eta) \\ \phi_0(\xi)\phi_2(\eta) \\ \phi_0(\xi)\phi_3(\eta) \\ \vdots \\ \phi_0(\xi)\phi_{p_z}(\eta) \end{array} \right] \begin{array}{l} \} \text{ node 1} \\ \} \text{ node 2} \\ \} \text{ node 3} \\ \} \text{ node 4} \\ \} \text{ edge } \gamma_1 \\ \} \text{ edge } \gamma_2 \\ \} \text{ edge } \gamma_3 \\ \} \text{ edge } \gamma_4 \end{array} \quad (3.17)$$

The two-dimensional basis functions, are based on the finite element basis functions

used for the finite element approximation in the  $x$ -direction (2.23). They are essentially a tensor product of one-dimensional basis functions for a quadrilateral element.

There are  $p_z + 1$  two-dimensional basis functions associated with the nodes of an edge, which is where the flux is being approximated: one for each vertex node and  $p_z - 1$  for the edge node. Therefore there are  $p_z + 1$  equations that must be solved to determine the coefficients  $\alpha_i$  in (3.16). The set of two-dimensional basis functions associated with the nodes of edge  $\gamma$  is a subset of the complete set given in (3.17 and defined as

$$\boldsymbol{\theta}^\gamma = \left[ \begin{array}{l} \theta_1^\gamma \\ \theta_2^\gamma \\ \theta_3^\gamma \\ \theta_4^\gamma \\ \vdots \\ \theta_{p_z+1}^\gamma \end{array} \right] \left. \begin{array}{l} \text{vertex nodes of } \gamma \\ \text{edge nodes of } \gamma \end{array} \right\} \quad (3.18)$$

The first four two-dimensional basis functions for edge  $\gamma_2$  are shown in Figure 3.2.

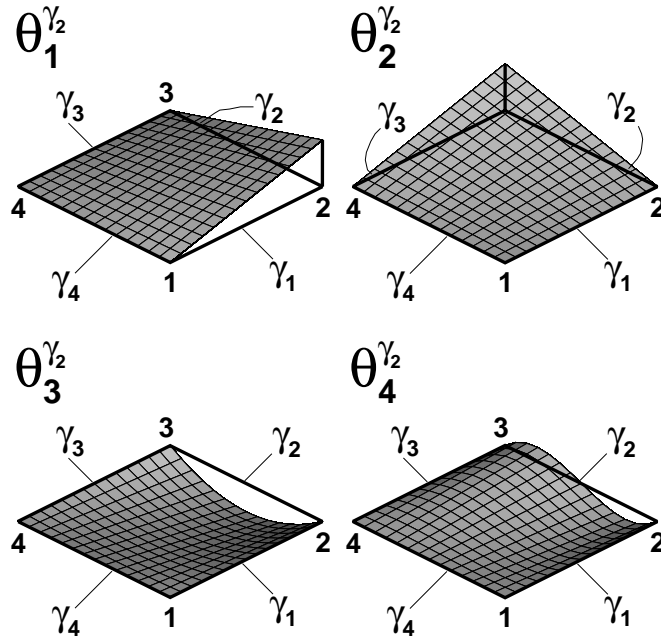


Figure 3.2: First four two-dimensional basis functions for edge  $\gamma_2$ .

The last term in (3.15) is an integral over the entire boundary of an element, and

can be written as a sum of integrals over each edge of the element:

$$F_{\Omega^e}(\theta_n) - B_{\Omega^e}(\hat{u}, \theta_n) - \left[ \int_{\gamma_1} q_b \theta_n^{\gamma_1} ds + \int_{\gamma_2} \hat{q}_{\Omega^e} \theta_n^{\gamma_2} ds + \int_{\gamma_3} q_t \theta_n^{\gamma_3} ds + \int_{\gamma_4} \hat{q}_{\Omega^e} \theta_n^{\gamma_4} ds \right] = 0 \quad (3.19)$$

where  $q_t$  is the heat flux specified on the top boundary of an element, and  $q_b$  is the heat flux specified on the bottom boundary of an element since  $\gamma_1$  and  $\gamma_3$  are coincident with  $\Gamma_N$ . Substitution of (3.16) into the boundary integral terms in (3.19) which include the approximate boundary flux,  $\hat{q}_{\Omega^e}$ , yields

$$\int_{\gamma} \hat{q}_{\Omega^e} \theta_n^{\gamma} ds = \int_{\gamma} \left( \sum_{i=1}^{p_z+1} \alpha_i \theta_i^{\gamma} \right) \theta_n^{\gamma} ds \quad \text{for } n = 1, \dots, p_z + 1 \quad (3.20)$$

This equation is true for each node,  $n$ , along  $\gamma$ , and can be rewritten in terms of a mass matrix as

$$\int_{\gamma} \hat{q}_{\Omega^e} \boldsymbol{\theta}^{\gamma} ds = \mathbf{M}_{\gamma} \boldsymbol{\alpha} \quad (3.21)$$

where  $\mathbf{M}_{\gamma}$  is the mass matrix along edge  $\gamma$  with entries

$$M_{ij} = \int_{\gamma} \theta_i \theta_j ds \quad \text{for } i, j = 1, \dots, p_z + 1 \quad (3.22)$$

In order to solve for the coefficients,  $\boldsymbol{\alpha}$ , (3.19) is written using (3.21) and moving the other terms to the right hand side. Due to the properties of the nodal basis functions, the sum of boundary integrals in (3.19) is simplified. For a nodal basis function at a vertex node, there are two edges along which the basis function is nonzero. Whereas for a nodal basis function at an edge node, there is only one edge along which the basis function is nonzero. This can be seen in Figure 3.2 where the first two plots show the basis functions for  $\gamma_2$ , and the third and fourth plots show the edge basis functions for  $\gamma_2$ . Each of the higher-order basis functions associated with the edge node is nonzero only on the edge containing the edge node. Using this information

about the nodal basis functions, and substituting (3.21) into (3.19) results in the following equations. For  $\gamma_2$ ,

$$\mathbf{M}_{\gamma_2} \boldsymbol{\alpha} = \left\{ \begin{array}{l} F_{\Omega^e}(\theta_1^{\gamma_2}) - B_{\Omega^e}(\hat{u}, \theta_1^{\gamma_2}) - \int_{\gamma_1} q_b \theta_1^{\gamma_2} ds \\ F_{\Omega^e}(\theta_2^{\gamma_2}) - B_{\Omega^e}(\hat{u}, \theta_2^{\gamma_2}) - \int_{\gamma_3} q_t \theta_2^{\gamma_2} ds \\ F_{\Omega^e}(\theta_3^{\gamma_2}) - B_{\Omega^e}(\hat{u}, \theta_3^{\gamma_2}) \\ \vdots \\ F_{\Omega^e}(\theta_{p_z+1}^{\gamma_2}) - B_{\Omega^e}(\hat{u}, \theta_{p_z+1}^{\gamma_2}) \end{array} \right\} \quad (3.23)$$

For  $\gamma_4$ ,

$$\mathbf{M}_{\gamma_4} \boldsymbol{\alpha} = \left\{ \begin{array}{l} F_{\Omega^e}(\theta_1^{\gamma_4}) - B_{\Omega^e}(\hat{u}, \theta_1^{\gamma_4}) - \int_{\gamma_1} q_b \theta_1^{\gamma_4} ds \\ F_{\Omega^e}(\theta_2^{\gamma_4}) - B_{\Omega^e}(\hat{u}, \theta_2^{\gamma_4}) - \int_{\gamma_3} q_t \theta_2^{\gamma_4} ds \\ F_{\Omega^e}(\theta_3^{\gamma_4}) - B_{\Omega^e}(\hat{u}, \theta_3^{\gamma_4}) \\ \vdots \\ F_{\Omega^e}(\theta_{p_z+1}^{\gamma_4}) - B_{\Omega^e}(\hat{u}, \theta_{p_z+1}^{\gamma_4}) \end{array} \right\} \quad (3.24)$$

Equations (3.23) and (3.24) are used to determine the approximate flux on each respective edge. The system of equations that must be solved to determine the coefficients  $\alpha$  will always have a unique solution since the mass matrix in these equations is positive definite.

### 3.3 Error Indicator

The error residual problem, shown in (3.4), can be used to approximate the error after choosing the method of approximating the true flux on the element boundaries and choosing an appropriate subspace  $V(\Omega^e)$ . The approach to approximating the error is the same as the approach used for the finite element approximation in Section 2.3.3. The approximation of the error in an element is

$$\hat{e} = \sum_{i=0}^{p_x+\sigma} \sum_{j=0}^{p_z+\sigma} \phi_i(x) \psi_j(z) b_{ij} \quad (3.25)$$

The Bubnov-Galerkin method is used so that the test functions,  $\hat{v}$ , are the same as the approximating functions,

$$\hat{v} = \chi_i \quad \text{for } i = 1, \dots, (p_x + 1 + \sigma) \times (p_z + 1 + \sigma) \quad (3.26)$$

Upon the substitution of (3.25) and (3.26) into (3.4), the approximate solution to the error residual problem for each element becomes a system of equations and can be written in matrix form as

$$B_{\Omega^e}(\hat{e}, \hat{v}) = F_{\Omega^e}(\hat{v}) - B_{\Omega^e}(\hat{u}, \hat{v}) + \int_{\partial\Omega^e} \hat{q}_{\Omega^e} \hat{v} ds \quad (3.27)$$

$$\mathbf{A}_e \mathbf{b} = \mathbf{F}_e \quad (3.28)$$

where  $\mathbf{A}_e$  represents the coefficient matrix based on the chosen subspace,  $V_{\Omega^e}$ ,  $\mathbf{b}$  is a vector of unknown constants, and  $\mathbf{F}_e$  is the load vector consisting of the element residual term and the boundary flux term. This system of equations is solved for the unknown coefficients,  $\mathbf{b}$ . The finite element solution satisfies the essential boundary condition on  $\Gamma_D$ . Therefore the error must be zero on this boundary. The penalty method, described in Chapter 2, is used to enforce this essential boundary condition in (3.28) for elements with boundaries coincident with  $\Gamma_D$ . This system of equations is singular except on those elements with a Dirichlet boundary where the error is set to zero. Singular value decomposition is used to find the the solution for  $\mathbf{b}$  which minimizes  $r \equiv |\mathbf{A} \mathbf{b} - \mathbf{F}|$  where the number  $r$  is called the residual of the solution [21]. In other words, the least-squares best compromise solution is found. The singular values are zeroed out when they are less than some tolerance. Therefore discretion in choosing a value for the tolerance must be used.

The error indicator for each element is obtained by calculating the energy norm of the error function. The energy norm is defined by the weak formulation

$$\varepsilon_{\Omega^e} = |||\hat{e}|||_{\Omega^e} \quad (3.29)$$

$$|||\hat{e}|||_{\Omega^e} = \sqrt{B_{\Omega^e}(\hat{e}, \hat{e})} = \left[ \int_{\Omega} (\boldsymbol{\kappa} \nabla \hat{e})^T \nabla \hat{e} d\Omega \right]^{\frac{1}{2}} \quad (3.30)$$

The global error estimate is calculated by computing the sum of the squares of the

local error indicators

$$\varepsilon = \left[ \sum_{\Omega^e} (\varepsilon_{\Omega^e})^2 \right]^{1/2} \quad (3.31)$$

### 3.4 Numerical Examples for the Total Error

The performance of the error estimates will be examined in this section. Example problems are chosen such that the exact solution is known. The problems are not meant to be realistic problems. The use of problems with exact solutions allows the actual error in the finite element solution to be computed and compared to the estimated error computed from (3.31). The first example problem has a smooth solution composed of a sine and a cosine function. The second example problem has a rough solution composed of an arctangent function. The finite element approximation for the first example will generally provide a better approximation (less error) than the second example problem for the same orders of approximation and mesh size because of the smoothness of the exact solution to the first example problem. The problems are developed using an inverse approach by first choosing a closed form solution,  $u$ , which satisfies the desired boundary conditions. Then the internal heat generation,  $Q$ , required to obtain the closed form solution is determined by substituting the exact solution into the heat conduction equation (2.6).

The examples will consider the two dimensional heat conduction problem shown in Figure 3.3. The heated plate has dimensions  $L$  by  $d$  with the following boundary conditions:

$$\begin{aligned} u &= 0 \quad \text{along the edges } x = 0 \text{ and } x = L \\ -k_z \frac{\partial u}{\partial z} &= 0 \quad \text{along } z = -\frac{d}{2} \\ -k_z \frac{\partial u}{\partial z} &= q_t \quad \text{along } z = \frac{d}{2} \end{aligned} \quad (3.32)$$

The plate has an internal heat source  $Q$ , and the heat load  $q_t$  applied along the

boundary at  $z = \frac{d}{2}$  is a function of  $x$ . The bottom of the plate is insulated, and the sides are held at a constant temperature of zero. For all results presented in this section,  $k_x = k_z = 1.4$ ,  $L = 1$ ,  $d = 1$ , and the value of  $\sigma = 1$  in (3.25) are used.

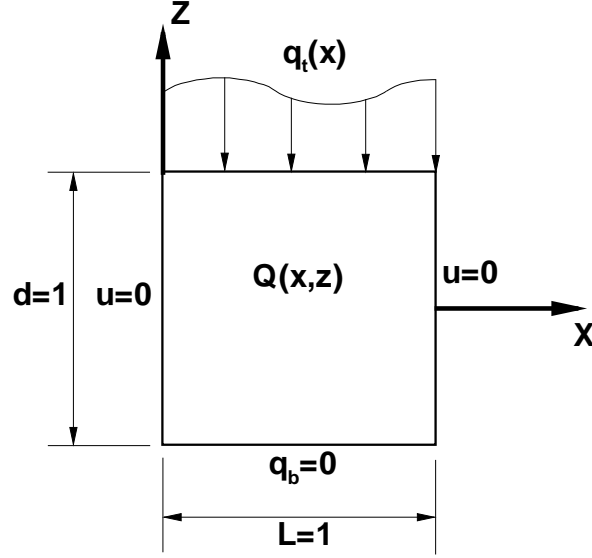


Figure 3.3: Two-dimensional plate for numerical examples.

### 3.4.1 Case I: Smooth Solution

The exact solution to the heat conduction equation (2.6) is chosen to be the analytic function

$$u = \alpha \left[ 1 - \cos\left(\frac{2\pi x}{L}\right) \right] \left[ \frac{-2d}{k_z \pi} \sin\left(\frac{\pi z}{2d} - \frac{\pi}{4}\right) \right] \quad (3.33)$$

This closed form solution satisfies the boundary conditions in (3.32) with the following heat load applied to the top boundary

$$q_t(x) = 1 - \cos\left(\frac{2\pi x}{L}\right) \quad (3.34)$$

The required internal heat source determined from (2.10) is

$$Q(x, z) = \frac{\alpha \pi \left[ k_z L^2 - (16d^2 k_x + k_z L^2) \cos\left(\frac{2\pi x}{L}\right) \right] \sin\left[\frac{\pi(d-2z)}{4d}\right]}{2dk_z L^2} \quad (3.35)$$

The contours of the exact solution for the heated square plate with  $\alpha = 10$  is shown in Figure 3.4. The solution is symmetric about the center line at  $x = 0.5$  and exhibits a very smooth behavior.

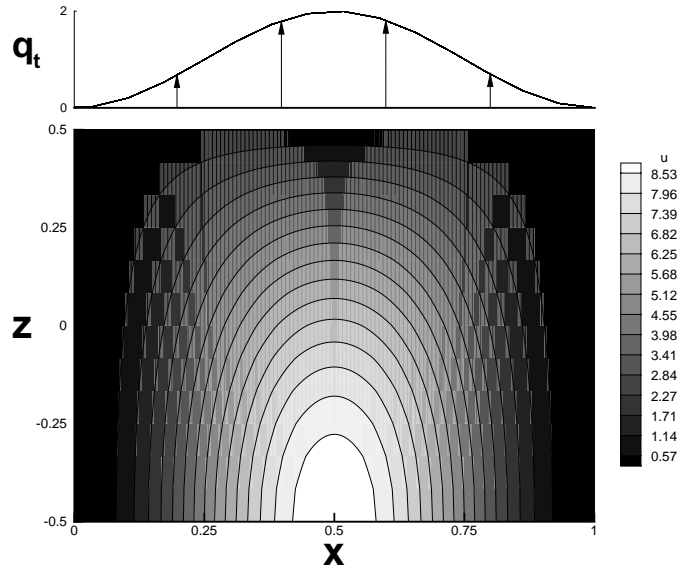


Figure 3.4: Exact solution for Case I.

The error estimate is computed using the average flux approximation, (3.9), and compared with the actual error in the energy norm in Figure 3.5. The graphs in Figure 3.5 show the rate of convergence of the error in the finite element approximation with respect to the length of the elements,  $h$ , in a uniform mesh. The error in the energy norm is plotted versus the inverse of the mesh size, which for a uniform mesh is the same as the number of elements, so that the error curves have a negative slope. Each graph represents a fixed particular value for  $p_x$ . Each line in a graph represents a different value of  $p_z$  varying from one to six. Each point on a particular line represents a uniform mesh of  $\frac{1}{h}$  one-dimensional elements. As  $p_x$  increases, the error converges faster (with fewer elements). The rate of convergence of the error, indicated by the slope of the solid line in each plot is equal to the value of  $p_x$ . For the constant part of a convergence curve where the lines level off, the hierarchical modelling error is dominating. In this region, refinement of the mesh does not improve the finite element

solution, and an increase in the chosen value for  $p_z$  is required to improve accuracy. When the hierarchical modelling error dominates, the estimated error (denoted by dashed lines in Figure 3.5) is only slightly larger than the actual error for all values of  $p_x$ . When the finite element error dominates, difference between the estimated error is significantly larger than the actual error, but exhibits correct rates of convergence. The discrepancy between the estimated and actual error is more pronounced for even-orders of  $p_x$ .

The error estimate computed using the equilibrated flux is compared to the actual error in Figure 3.6. Comparing Figure 3.6 with Figure 3.5 shows that the equilibrated flux method provides more accurate error estimates, particularly when the error is dominated by the finite element approximation error. The estimated and actual errors using the equilibrated flux method are virtually indistinguishable for all values of  $p_x$ ,  $p_z$ , and mesh size.

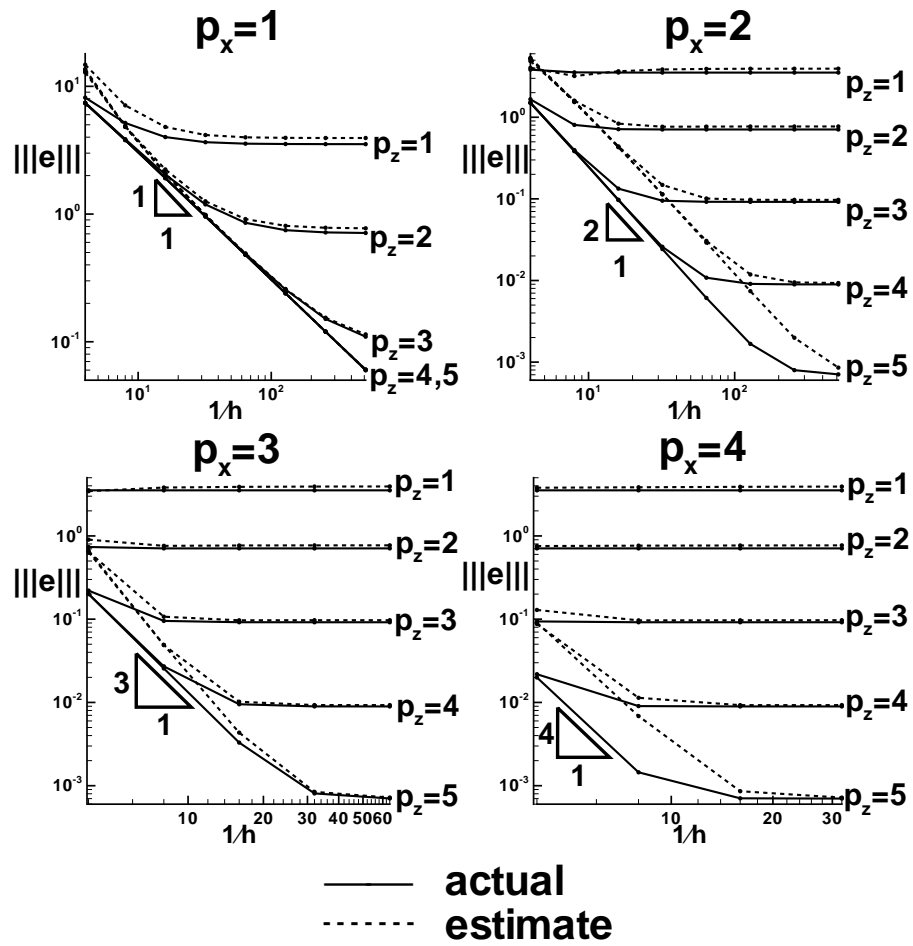


Figure 3.5: Error for Case I using the average flux method.

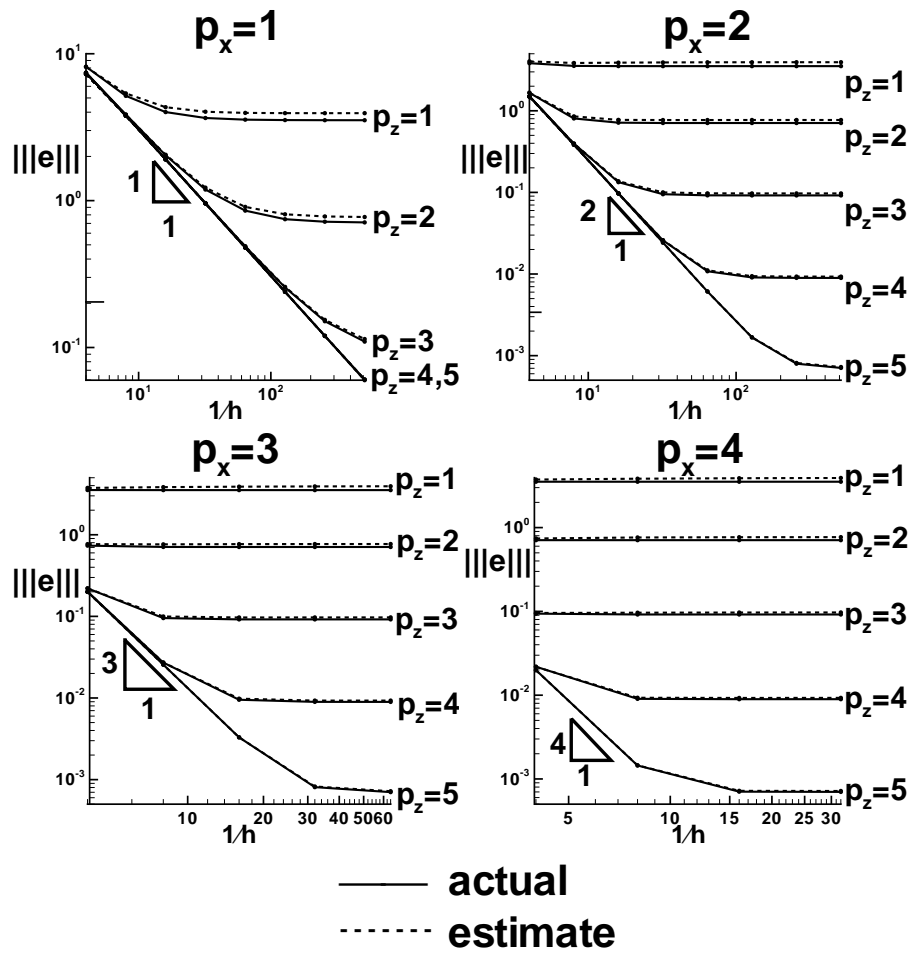


Figure 3.6: Error for Case I using the equilibrated flux method.

### 3.4.2 Case II: Rough Solution

The performance of the error estimates for a problem with a rough solution will now be examined. The closed form solution is given by

$$u = \alpha(L - x) [\arctan[\alpha(x - x_0)] + \arctan(\alpha x_0)] \left[ \frac{-2d}{k_z \pi} \sin\left(\frac{\pi z}{2d} - \frac{\pi}{4}\right) \right] \quad (3.36)$$

This solution satisfies the boundary conditions (3.32) with the applied heat load along the top of the plate defined by

$$q_t(x) = \alpha(L - x) [\arctan[\alpha(x - x_0)] + \arctan(\alpha x_0)] \quad (3.37)$$

The internal heat source required to deliver the solution in (3.36) is determined from (2.6) to be

$$Q(x, z) = \frac{\alpha \pi (L - x) [\arctan[\alpha(x - x_0)] + \arctan[\alpha x_0]] \sin\left(\frac{\pi}{4} - \frac{\pi z}{2d}\right)}{2d} - \frac{2\alpha d k_x \left[ -\frac{2\alpha \sin\left(\frac{\pi}{4} - \frac{\pi z}{2d}\right)}{\pi[1 + \alpha^2(x - x_0)^2]} - \frac{2\alpha^3(L - x)(x - x_0) \sin\left(\frac{\pi}{4} - \frac{\pi z}{2d}\right)}{\pi[1 + \alpha^2(x - x_0)^2]^2} \right]}{k_z} \quad (3.38)$$

where  $\alpha = 30$  and  $x_0 = 0.3$ . This exact solution has steep gradients in the  $x$ -direction in the vicinity of  $x = x_0$  as seen in the contours of the exact solution shown in Figure 3.7.

The actual error is compared with the estimated errors using the average and equilibrated boundary flux methods in Figures 3.8 and 3.9. The actual error in the energy norm is not as well behaved as in Case I because the solution for this case is not as smooth. Smaller mesh sizes are required to reach the expected rate of convergence of  $p_x$  [4] as shown in Figures 3.5 and 3.6. The error estimates obtained using the average flux method are much larger than the actual error. In comparison of the error estimates obtained using the average and equilibrated flux methods for Case II, the equilibrated flux method provides noticeably better error estimates than the average flux method. A contour plot of the pointwise error in a finite element

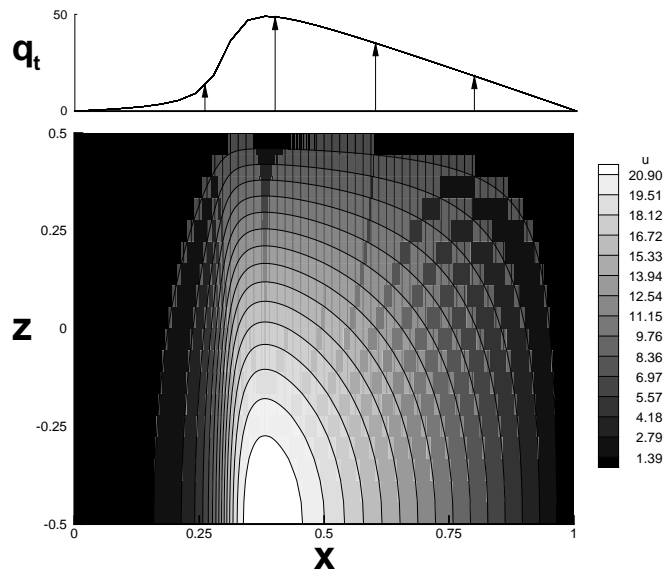


Figure 3.7: Exact solution for Case II.

solution obtained with 32 elements and  $p_x = p_z = 2$ , shown in Figure 3.10, shows that the greatest errors occur after  $x = x_0$  where the steep gradients occur. The element error indicators, obtained with the average and equilibrated flux methods are compared with the actual element error in Figures 3.11 and 3.12. The actual and estimated errors in the finite element solution for  $p_x = p_z = 2$  with 32 elements are shown. For this case, the global error for the equilibrated flux provides a much better estimate of the error than the average flux method. The average flux method severely over-estimates the error for each element in the region near  $x = x_0$ , while the equilibrated flux method provides an accurate indicator of the error for each element.

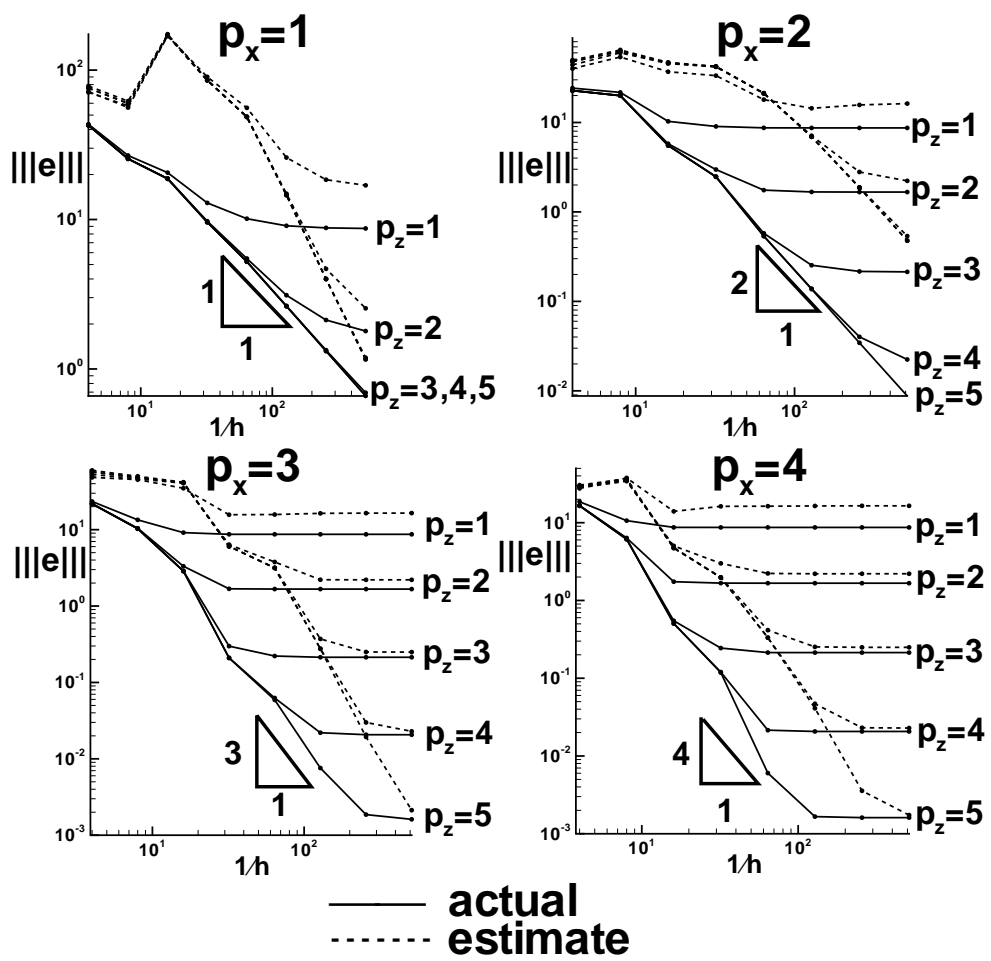


Figure 3.8: Error for Case II using the average flux method.

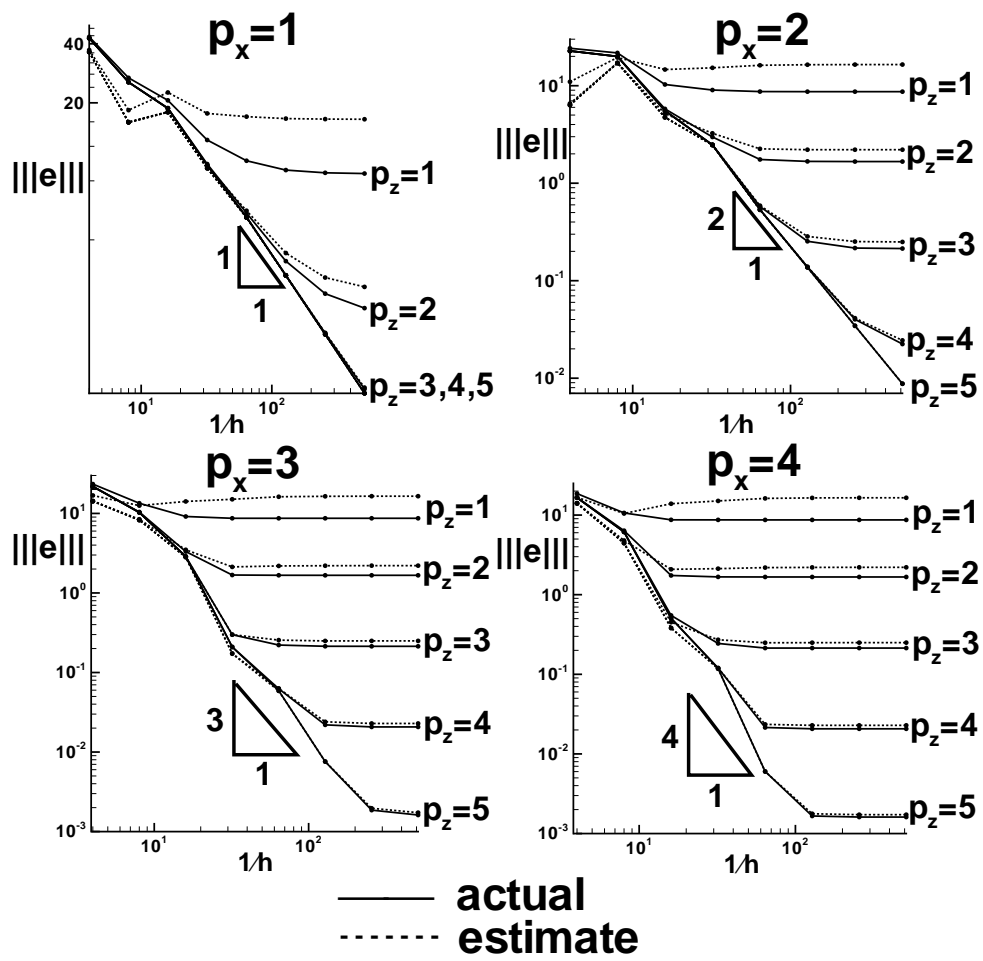


Figure 3.9: Error for Case II using the equilibrated flux method.

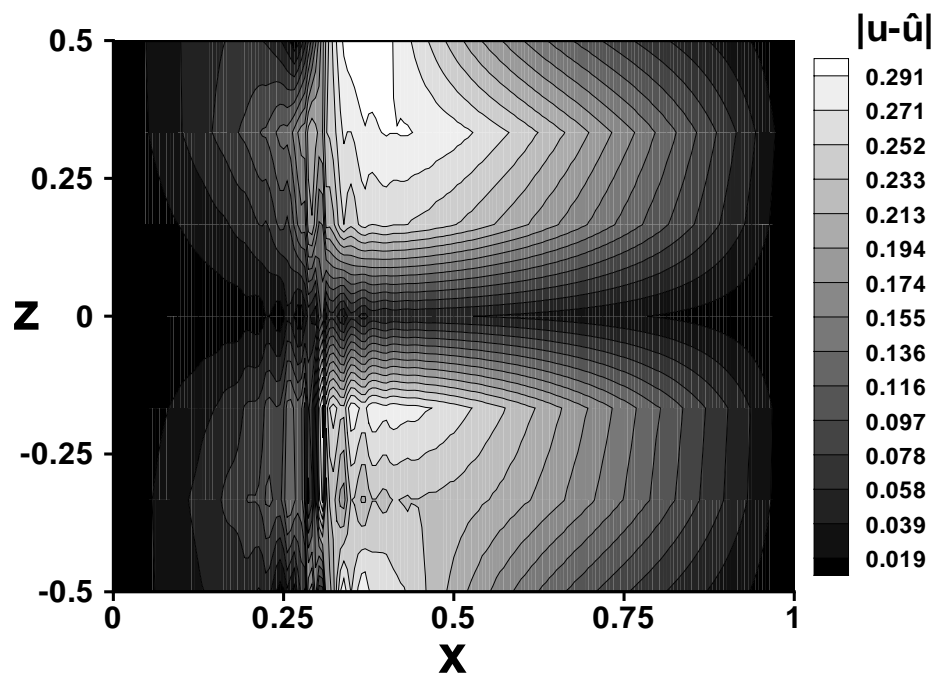


Figure 3.10: Pointwise error in the finite element solution for Case II using 32 elements with  $p_x = p_z = 2$ .

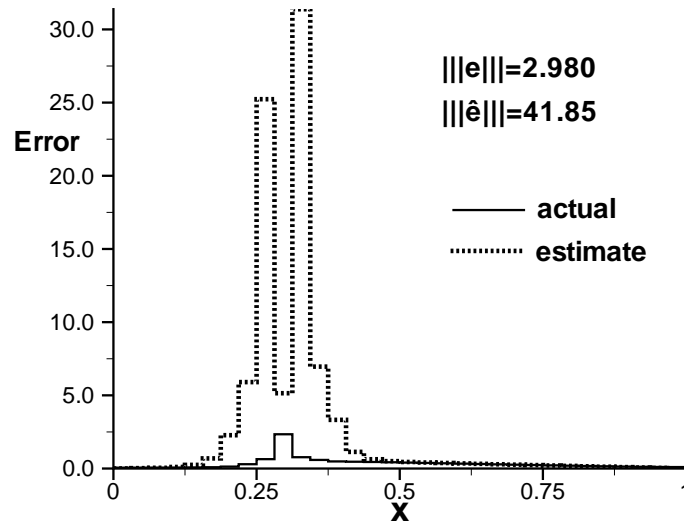


Figure 3.11: Element error indicators for Case II solution using 32 elements with  $p_x = p_z = 2$  using the average flux method.

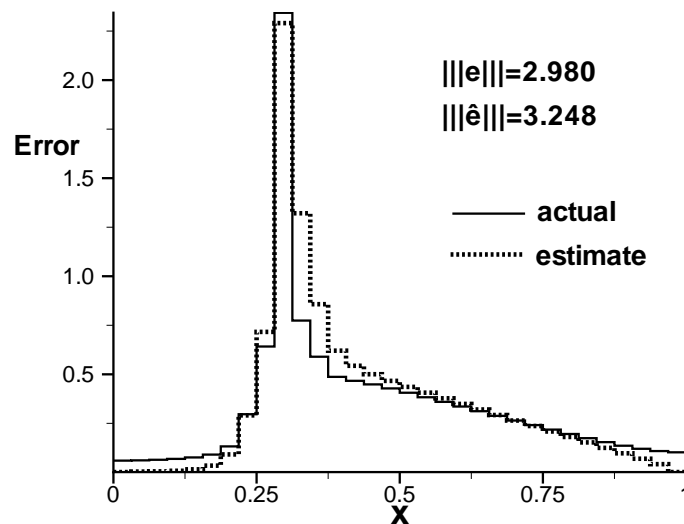


Figure 3.12: Element error indicators for Case II solution using 32 elements with  $p_x = p_z = 2$  using the equilibrated flux method.

### 3.5 Directional Error Indicators

The element error indicator described in the previous section gives an estimate of the accuracy of the approximate solution on each element. There are various approaches to improve the finite element solution. Some of these techniques include refining the mesh, increasing the order of the approximation, and using different basis functions. When using the hierarchical modelling approach, the through-thickness polynomial degree, the mesh size, and the in-plane (or  $x$ -direction) polynomial degree are parameters which will affect the accuracy of the solution. A directional error indicator provides an estimate of the error in the hierarchical model and finite element approximation separately. The directional error indicator indicates which parameters to change to efficiently improve the approximate solution. According to Figure 3.6, the error in approximating the solution in the  $z$ -direction with a polynomial of order  $p_z$  is dominant at the points where the lines are flat. In this circumstance, increasing the value of  $p_z$  will improve the approximate solution while refinement of the mesh will not. If the approximate solution has an error which is located on the part of the lines where the slope is  $p_x$ , then the error in the finite element method is dominant, and refinement of the mesh would be the appropriate choice to reduce the error in the solution. Directional error indicators could be used to distinguish between these circumstances by determining which contribution to the error, the hierarchical model or the finite element method, is the largest.

The error in the solution is composed of the error in the hierarchical model,  $e_{Model}$ , and the error in the finite element approximation of the hierarchical model,  $e_{FE}$ .

$$e_{Model} = u - u_{Model} \quad (3.39)$$

$$e_{FE} = u_{Model} - \hat{u} \quad (3.40)$$

The solution  $u_{Model}$  is the exact solution to the hierarchical model, that is the exact

solution to the system of differential equations resulting from the assumption that the solution is a polynomial of  $p_z$  in the through-thickness direction of the entire domain. The finite element error is associated with the polynomial approximation of degree  $p_x$  in the  $x$ -direction. The total error can be expressed as the sum of the modelling error and the finite element approximation error

$$\begin{aligned}
e &= u - \hat{u} \\
e &= u - u_{Model} + u_{Model} - \hat{u} \\
e &= e_{Model} + e_{FE}
\end{aligned} \tag{3.41}$$

The energy norm, defined in (3.30) from the weak formulation, is used to measure the error in the approximate solution

$$|||e|||^2 = B(e, e) \tag{3.42}$$

Substituting the definition of  $e$  in (3.41) into (3.42) and expanding yields

$$\begin{aligned}
B(e, e) &= B(e_{Model} + e_{FE}, e_{Model} + e_{FE}) \\
B(e, e) &= B(e_{Model}, e_{Model}) + B(e_{FE}, e_{FE}) + B(e_{Model}, e_{FE}) + \\
&\quad B(e_{FE}, e_{Model})
\end{aligned} \tag{3.43}$$

$B(\cdot, \cdot)$  is symmetric, and the modelling error is orthogonal to the finite element approximation error [5], meaning

$$B(e_{Model}, e_{FE}) = 0 \tag{3.44}$$

$$B(e_{FE}, e_{Model}) = 0 \tag{3.45}$$

Using (3.44) and (3.45), the last two terms in the definition of the energy norm of the total error in (3.43) become zero, so that

$$\begin{aligned}
B(e, e) &= B(e_{Model}, e_{Model}) + B(e_{FE}, e_{FE}) \\
|||e|||^2 &= |||e_{Model}|||^2 + |||e_{FE}|||^2
\end{aligned} \tag{3.46}$$

This equation shows how the directional errors are related to the total error.

The total element error for the model problem is approximated using the following polynomial, as discussed in Section 3.3,

$$\hat{e} = \sum_{i=0}^{p_x+\sigma} \sum_{j=0}^{p_z+\sigma} \phi_i(x)\psi_j(z)b_{ij} \quad \sigma \geq 1 \quad (3.47)$$

Recall that  $\sigma$  must be greater or equal to 1 to ensure that the result for the error estimate is nontrivial. The finite element error is the error in the solution which is controlled by the mesh size and the polynomial order in the  $x$ -direction,  $h$  and  $p_x$ . The modelling error is controlled by the through-thickness polynomial order,  $p_z$ . To approximate each of the directional error indicators, the opposing  $\sigma$  is set to zero in (3.47). The directional error polynomial approximations are

$$\begin{aligned} \hat{e}_{FE} &= \sum_{i=0}^{p_x+\sigma} \sum_{j=0}^{p_z} \phi_i(x)\psi_j(z)b_{ij} \\ \hat{e}_{Model} &= \sum_{i=0}^{p_x} \sum_{j=0}^{p_z+\sigma} \phi_i(x)\psi_j(z)c_{ij} \end{aligned} \quad (3.48)$$

Using each of these approximations separately in the element residual error equation (3.28) with either the average and equilibrated flux methods described in Sections 3.2.1 and 3.2.2, the approximate solution for each of the errors can be found. The directional error indicators are computed using the energy norm of the approximate error functions:

$$|||e|||_{\Omega}^2 = B(e, e) = \sum_{\Omega^e} B_{\Omega^e}(e, e) \quad (3.49)$$

$$\varepsilon_{FE} = |||\hat{e}_{FE}|||_{\Omega} = \sqrt{B(\hat{e}_{FE}, \hat{e}_{FE})} = \sqrt{\sum_{\Omega^e} B_{\Omega^e}(\hat{e}_{FE}, \hat{e}_{FE})} \quad (3.50)$$

$$\varepsilon_{Model} = |||\hat{e}_{Model}|||_{\Omega} = \sqrt{B(\hat{e}_{Model}, \hat{e}_{Model})} = \sqrt{\sum_{\Omega^e} B_{\Omega^e}(\hat{e}_{Model}, \hat{e}_{Model})} \quad (3.51)$$

### 3.6 Numerical Examples for the Directional Error Estimates

Results for Case I and II are examined using the directional error indicators. The equilibrated flux method is used to approximate the element boundary fluxes. Figure 3.13 shows the actual error, the model error estimate, and the finite element error estimate plotted versus the inverse of the mesh size for the problem in Case I. The  $p_z$  value is varied with uniform mesh refinements for a fixed  $p_x$  value. The graphs in Figure 3.13 show that the estimated error in the finite element approximation (denoted by triangles) has a slope of  $p_x$ , and follows the convergence rate of the actual error. The actual hierarchical modelling error for each value of  $p_z$  is determined by the horizontal portion of the actual error line. The estimated hierarchical modelling error is accurate for sufficiently small mesh sizes, which are determined by the value of  $p_x$ . At each point on each line, the most effective method of improving the approximate solution is determined by which error indicator is larger.

The directional error indicators for Case II are shown in Figure 3.14. The actual error, model error estimate, and finite element error estimate are plotted versus the inverse of the mesh size. The actual error norms are not as well behaved as in Case I due to the roughness of the problem, however, the finite element error is accurately predicted by the directional error estimates. The estimated hierarchical modelling error is slightly higher than the actual hierarchical modelling error for low values of  $p_z$  and for large mesh sizes. The results of these examples show that the directional error indicators accurately determined which error dominates, the model or the finite element error, for a smooth and a rough solution. Knowledge of which error is dominant in the approximate solution indicates the most effective way to improve the approximate solution.

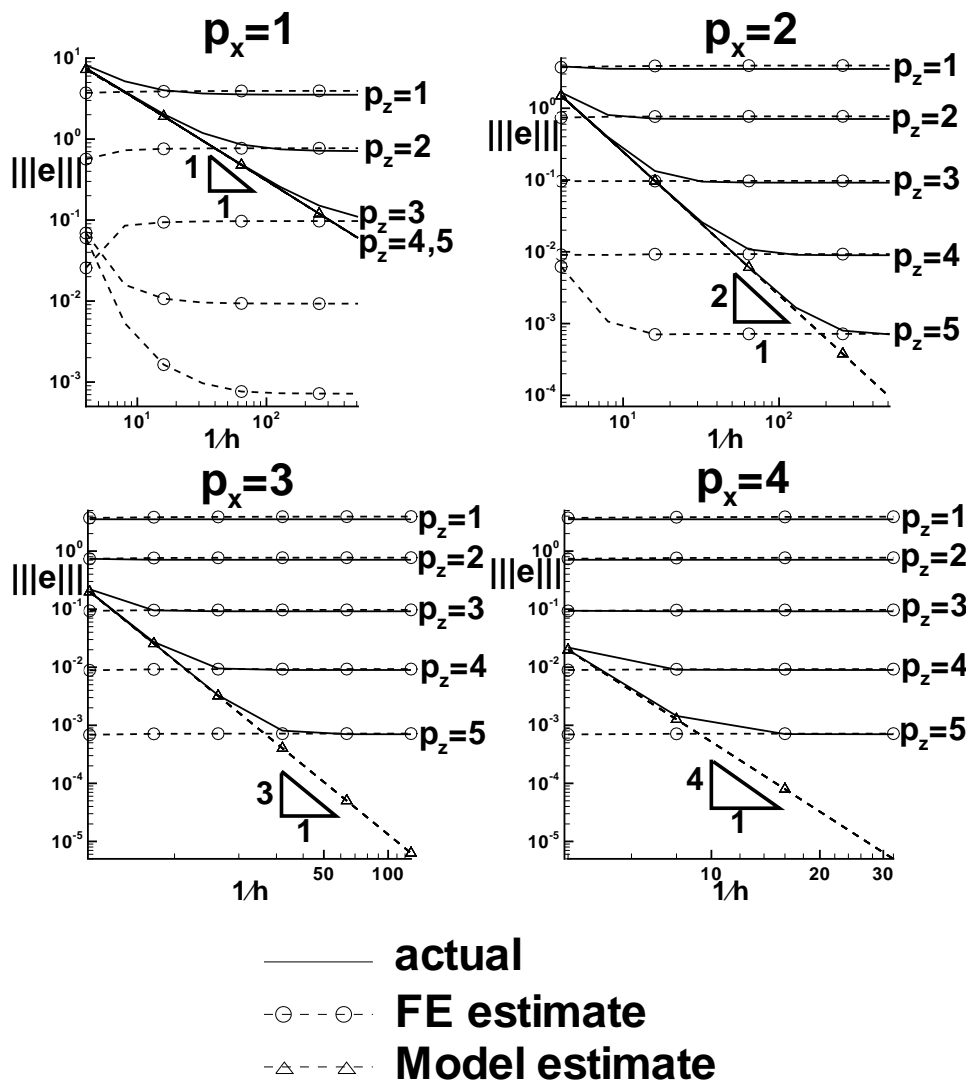


Figure 3.13: Directional error estimation for Case I using the equilibrated flux method.

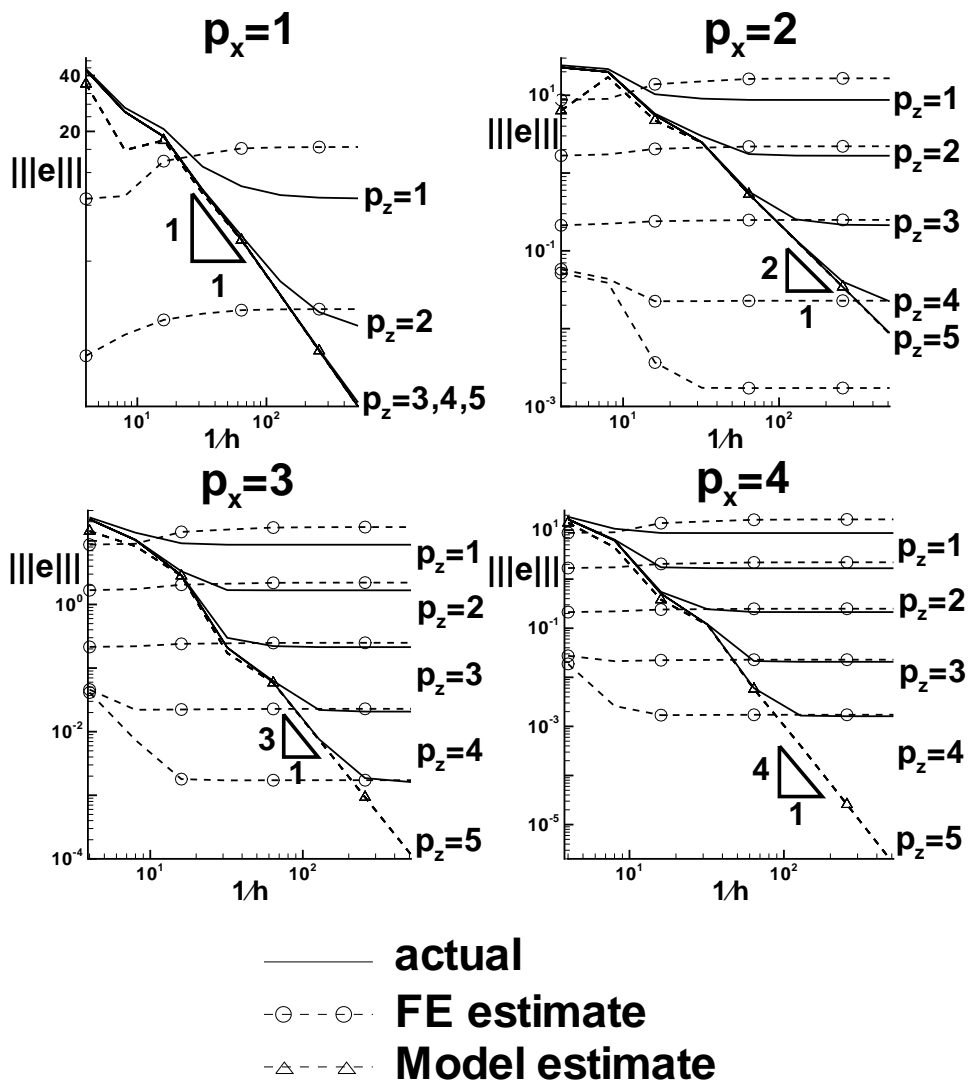


Figure 3.14: Directional error estimation for Case II using the equilibrated flux method.

# Chapter 4

## Extension to Multi-layered Materials

Structural concepts for aerospace vehicles often consist of panels made of multi-layer materials. Examples include skins of composite laminates or metallic thermal protection systems. Accurate and efficient analysis methods are required to aid in the design of such concepts. Hierarchical modelling, p-version finite elements, and error estimation are extended to multi-layered materials in this chapter.

### 4.1 Boundary Value Problem

Section 2.1 presents the boundary value problem for a single layer. The two-dimensional domain for a multi-layered material for a plate with length  $L$ , thickness  $d$ , and  $n_L$  layers of material is shown in Figure 4.1. The boundary value problem must be satisfied by the solution for the temperature in each layer,  $u_i$ , with the boundary conditions described on the boundary of the global domain:

$$\begin{aligned} -\nabla^T(\boldsymbol{\kappa}_i \nabla u_i) &= Q \quad i = 1, \dots, n_L \\ -(\boldsymbol{\kappa}_i \nabla u_i)^T \mathbf{n}_\Omega &= q_s \quad \text{on } \Gamma_N \\ u_i &= u_s \quad \text{on } \Gamma_D \end{aligned} \tag{4.1}$$

For layered materials, continuity at the boundaries of the layers must also be satisfied.

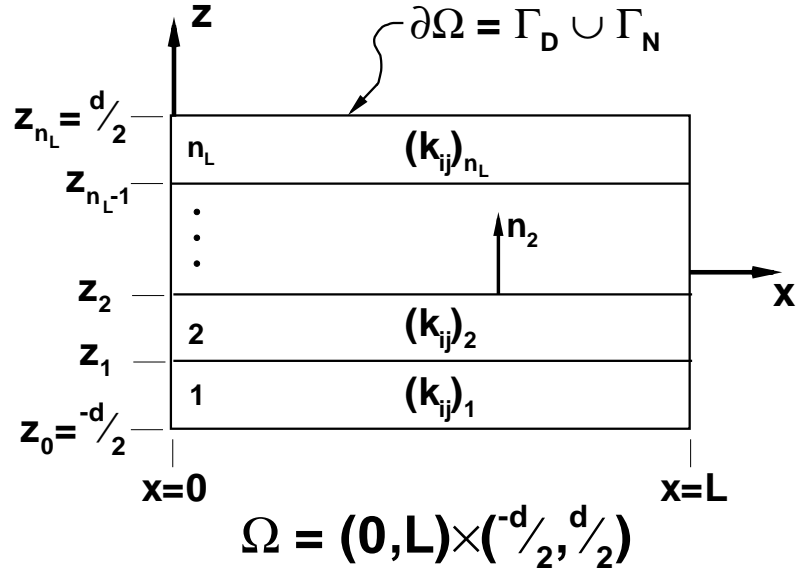


Figure 4.1: Two-dimensional domain for a multi-layered material.

At each layer interface, the temperature and the heat flux are required to be equal

$$\left. \begin{aligned} u_i|_{z_i} &= u_{i+1}|_{z_i} \\ -(\boldsymbol{\kappa}_i \nabla u_i)^T \mathbf{n}_i|_{z_i} &= -(\boldsymbol{\kappa}_{i+1} \nabla u_{i+1})^T \mathbf{n}_{i+1}|_{z_i} \end{aligned} \right\} \quad i = 1, \dots, n_L - 1 \quad (4.2)$$

where  $i$  denotes the layer of interest,  $z_i$  represents the  $z$ -coordinate of the layer interface, and the outward unit normal vector to the boundary of layer  $i$  is  $\mathbf{n}_i$ .

## 4.2 Finite Element Method for Multi-Layers

The finite element method used in this research for materials with multiple layers is similar to the method described in Chapter 2. The through-thickness direction is modelled by a polynomial function of degree  $p_z$ , reducing the spatial dimension of the domain by one, a mesh is created for the dimensionally-reduced domain, and the p-version finite element method is used to complete the approximation. The thermal conductivity for the orthotropic multi-layered materials is assumed in this research to be a piecewise constant function in the through-thickness direction,

$$\boldsymbol{\kappa}_i = \begin{bmatrix} (k_x)_i & 0 \\ 0 & (k_z)_i \end{bmatrix} \quad (4.3)$$

### 4.2.1 Weak Formulation

The weak form of (4.1) is constructed by multiplying by a test function and integrating by parts. The test function is required to be zero on  $\Gamma_D$ .

$$\int_{\Omega} (\boldsymbol{\kappa} \nabla u)^T \nabla v \, d\Omega = \int_{\Omega} Qv \, d\Omega - \int_{\Gamma_N} q_s v \, ds \quad (4.4)$$

In abstract form, the problem is to find  $u \in V(\Omega)$  such that  $u = u_s$  on  $\Gamma_D$  and

$$B(u, v) = L(v) \quad \text{for all admissible } v \in V(\Omega) \quad (4.5)$$

The subscript  $i$  has been dropped in (4.4) and (4.5) with the understanding that the thermal conductivity is a piecewise constant function of  $z$ , and the exact solution is piecewise defined on each layer. The hierarchical modelling combined with p-version finite element method is used to approximate the solution to (4.5). The p-version method for multi-layers is identical to the method described in Section 2.3.2 for a single layer, where the basis functions,  $\boldsymbol{\phi}$ , in (2.23) are used. However, since one approximate solution is computed for all layers in each element, the hierarchical modelling method is modified by choosing a more efficient set of through-thickness basis functions to approximate the exact solution using piecewise polynomials.

### 4.2.2 Optimal Hierarchical Model

Piecewise constant thermal conductivities in the boundary value problem in (4.1) result in a piecewise exact solution in the through-thickness direction. The work of Vogelius and Babuska [5] shows that the optimal choice of basis functions for hierarchical modelling of the boundary value problem (4.1) are piecewise polynomials. The choice of basis functions are optimal in the sense that the approximate solution converges to the exact solution at the expected rate as the polynomial order,  $p_z$ , approaches infinity and as the plate thickness,  $d$ , approaches zero. The basis functions for hierarchical modelling in single-layered materials are referred to as homogenized

basis functions. The set of optimal basis functions,  $\hat{\boldsymbol{\psi}}$ , is constructed by scaling the odd-degree through-thickness homogenized basis functions,  $\boldsymbol{\psi}$ , by the conductivity of each layer and shifting the resulting polynomial to enforce continuity at the layer interfaces:

$$\begin{aligned} \hat{\psi}_{2j} &= \psi_{2j} \quad j = 0, \dots, \frac{p_z}{2} \\ \hat{\psi}_{2j-1} &= \begin{cases} \hat{\psi}_{2j-1}^1 & -1 \leq \eta \leq \eta_1 \\ \hat{\psi}_{2j-1}^2 & \eta_1 \leq \eta \leq \eta_2 \\ \vdots \\ \hat{\psi}_{2j-1}^{n_L} & \eta_{n_L-1} \leq \eta \leq 1 \end{cases} \quad j = 1, \dots, \frac{p_z}{2} \end{aligned} \quad (4.6)$$

where

$$\begin{aligned} \hat{\psi}_{2j-1}^1 &= \frac{1}{(k_z)_1} \psi_{2j-1} \\ \hat{\psi}_{2j-1}^i &= \frac{1}{(k_z)_i} (\psi_{2j-1} - \psi_{2j-1}(\eta_{i-1})) + c_i \quad i = 2, \dots, n_L \\ c_2 &= \frac{1}{(k_z)_1} \psi_{2j-1}(\eta_1) \\ c_{i+1} &= c_i + \frac{1}{(k_z)_i} (\psi_{2j-1}(\eta_i) - \psi_{2j-1}(\eta_{i-1})) \quad i = 2, \dots, n_L - 1 \end{aligned} \quad (4.7)$$

and  $i$  is the layer of interest,  $\hat{\psi}_{2j-1}^i$  is the optimal polynomial of degree  $2j - 1$  in the  $i^{\text{th}}$  layer, and  $\psi_j$  are given in (2.19). These basis functions provide more accurate approximations for layered materials than the single layer through-thickness basis functions described in Section 2.3.1. An example of these basis functions are shown in Figure 4.2 for a three layer material with  $(k_z)_1 = 1$ ,  $(k_z)_2 = 10$ , and  $(k_z)_3 = 1$  for the polynomials of degree 0 through 7. Note that the odd degree basis functions have discontinuous derivatives at the layer interfaces.

### 4.2.3 Element Equations

The finite element solution,  $\hat{u}$ , on an element is written as a linear combination of the basis functions

$$\hat{u}|_{\Omega^e} = \sum_{i=0}^{p_x} \sum_{j=0}^{p_z} \phi_i(\xi) \hat{\psi}_j(\eta) a_{ij} = (\boldsymbol{\phi} \otimes \hat{\boldsymbol{\psi}})^T \mathbf{a}_e = \hat{\boldsymbol{\chi}}^T \mathbf{a}_e \quad (4.8)$$

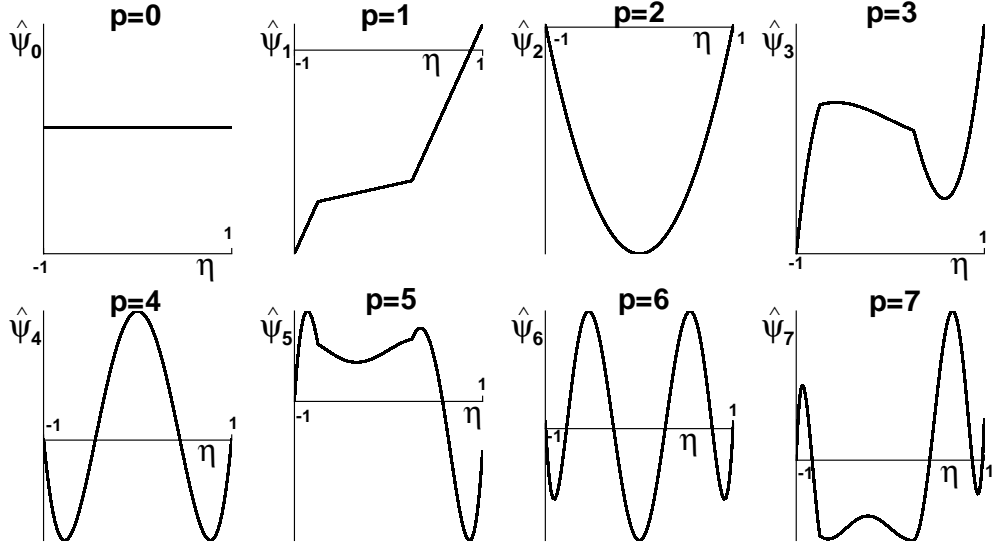


Figure 4.2: The optimal basis functions for a three layer material with  $(k_z)_1 = 1$ ,  $(k_z)_2 = 10$ , and  $(k_z)_3 = 1$ .

The variational problem in (4.4) is written as a sum of integrals over each element

$$\sum_{e=1}^N \int_{\Omega^e} (\boldsymbol{\kappa} \nabla u)^T \nabla v \, d\Omega^e = \sum_{e=1}^N \int_{\Omega^e} Qv \, d\Omega^e - \int_{\partial\Omega^e \cap \Gamma_N} q_s \, ds \quad (4.9)$$

The Bubnov-Galerkin method chooses the test function to be the same as the approximating functions, and substituting (4.8) for  $u$  and  $\hat{\chi}_i, i = 1, \dots, (p_x + 1) \times (p_z + 1)$  for  $v$  into (4.9) yields a system of equations which can be written in matrix form as

$$\left( \sum_{e=1}^N \mathbf{A}_{\Omega^e} \right) \mathbf{a} = \sum_{e=1}^N \mathbf{F}_{\Omega^e} \quad (4.10)$$

where the element matrix and the load vector are defined as

$$\begin{aligned}
\mathbf{A}_{\Omega^e} &= \int_{\Omega^e} \nabla \hat{\chi} (\boldsymbol{\kappa} \nabla \hat{\chi})^T d\Omega^e \\
&= \sum_{i=1}^{n_L} \int_{x_0}^{x_1} \int_{z_{i-1}}^{z_i} \nabla \hat{\chi} (\boldsymbol{\kappa} \nabla \hat{\chi})^T dz dx \\
&= \int_{x_0}^{x_1} \frac{\partial \phi}{\partial x} \frac{\partial \phi^T}{\partial x} dx \otimes \sum_{i=1}^{n_L} \int_{z_{i-1}}^{z_i} (k_x)_i \hat{\boldsymbol{\psi}} \hat{\boldsymbol{\psi}}^T dz + \\
&\quad \int_{x_0}^{x_1} \phi \phi^T dx \otimes \sum_{i=1}^{n_L} \int_{z_{i-1}}^{z_i} (k_z)_i \frac{\partial \hat{\boldsymbol{\psi}}}{\partial z} \frac{\partial \hat{\boldsymbol{\psi}}^T}{\partial z} dz
\end{aligned} \tag{4.11}$$

$$\begin{aligned}
\mathbf{F}_{\Omega^e} &= \int_{\Omega^e} Q \hat{\chi} d\Omega^e - \int_{\partial\Omega^e \cap \Gamma_N} q_s \hat{\chi} ds \\
&= \sum_{i=1}^{n_L} \int_{x_0}^{x_1} \int_{z_{i-1}}^{z_i} Q \hat{\chi} dz dx - \int_{\partial\Omega^e \cap \Gamma_N} q_s \hat{\chi} ds
\end{aligned} \tag{4.12}$$

### 4.3 Multi-Layer *A Posteriori* Error Estimation

The element residual method is applied to multi-layered materials. A local boundary value problem for the error is developed, and the equilibrated flux method is modified for application to multi-layered materials. The solution to the error equation is approximated and used in the definition of the energy norm to compute the error indicator for each element. Numerical results are presented for multi-layered materials. According to the literature search performed, numerical results for applying the element residual method to multi-layered materials have not yet been presented.

#### 4.3.1 Element Residual Method

The weak form of the local error residual problem derived in Section 3.1 is used for the multi-layer problem.

$$\begin{aligned}
\int_{\Omega^e} (\boldsymbol{\kappa} \nabla e)^T \nabla v d\Omega^e &= \int_{\Omega^e} Q v d\Omega^e - \int_{\Omega^e} (\boldsymbol{\kappa} \nabla \hat{u})^T \nabla v d\Omega^e + \int_{\partial\Omega^e} (\boldsymbol{\kappa} \nabla u)^T \mathbf{n}_{\Omega^e} v ds \\
B_{\Omega^e}(e, v) &= F_{\Omega^e}(v) - B_{\Omega^e}(\hat{u}, v) + \int_{\partial\Omega^e} (\boldsymbol{\kappa} \nabla u)^T \mathbf{n}_{\Omega^e} v ds \\
e &= 0 \quad \text{on } \Gamma_D
\end{aligned} \tag{4.13}$$

The last term in the variational form of the element error residual problem is the exact flux, and an approximation must be made since the exact solution is not known. The

next section discusses the modified equilibrated flux method of approximating the boundary fluxes on an interior element boundary for multi-layer problems.

### 4.3.2 Equilibrated Boundary Flux Approximation

The equilibrated flux method is used to approximate the element boundary flux, but the method must be modified for multi-layered materials. The exact flux in the  $x$ -direction is discontinuous along the boundary of an element (not across the boundary) in the through-thickness direction because of the piecewise constant thermal conductivity. Figure 4.3 shows an example of the discontinuous boundary flux on an element with four layers. Therefore the method chosen to approximate the exact boundary flux should also be discontinuous. To develop an equilibrated discontinuous flux, the

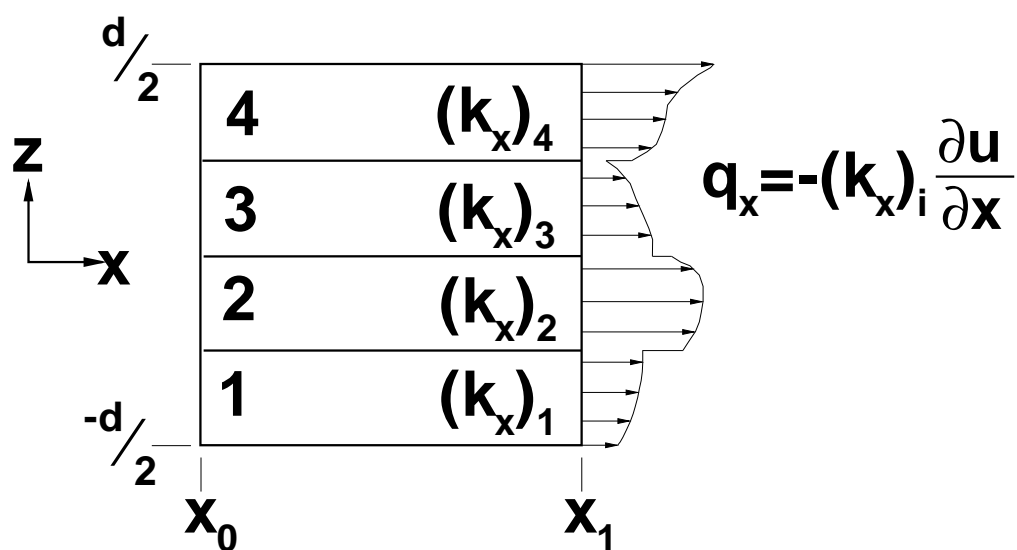


Figure 4.3: Example of a discontinuous exact boundary flux in the  $x$ -direction on a four layer element.

equilibrated flux method is modified by defining the approximate flux on each element as

$$\hat{q}_{\Omega^e} = \bar{q}_{\Omega^e} + \tilde{q}_{\Omega^e} \quad (4.14)$$

where  $\bar{q}_{\Omega^e}$  is the average flux and  $\tilde{q}_{\Omega^e}$  is the deviation from the average required to equilibrate the flux. The average flux is discontinuous since it is computed by averaging the finite element fluxes from neighboring elements as described in Section 3.2.1

$$\bar{q}_{\Omega^e} = \frac{1}{2} (\boldsymbol{\kappa} \nabla \hat{u}_{\Omega^e} |_{\partial\Omega^e} + \boldsymbol{\kappa} \nabla \hat{u}_{\Omega^e} |_{\partial\Omega^e})^T \mathbf{n}_{\Omega^e} \quad (4.15)$$

The equilibrium condition for the equilibrated flux in a single layer is used to find  $\tilde{q}_{\Omega^e}$ . The definition for  $\hat{q}_{\Omega^e}$  in (4.14) is substituted into (3.15)

$$F_{\Omega^e}(\theta_n) - B_{\Omega^e}(\hat{u}, \theta_n) - \int_{\partial\Omega^e} \bar{q}_{\Omega^e} \theta_n \, ds - \int_{\partial\Omega^e} \tilde{q}_{\Omega^e} \theta_n \, ds = 0 \quad \text{for } n = 1, \dots, n_\gamma \quad (4.16)$$

For the boundary of an element that coincides with  $\Gamma_N$ ,

$$\bar{q}_{\Omega^e} + \tilde{q}_{\Omega^e} = q_s \quad \text{on } \partial\Omega^e \cap \Gamma_N \quad (4.17)$$

The approach to solve (4.16) for  $\tilde{q}_{\Omega^e}$  is the same as described in Section 3.2.2 to solve (3.15). The deviation from the average flux,  $\tilde{q}_{\Omega^e}$ , is written in terms of the nodal basis functions,  $\theta_n$ , (see (3.18)) with the same through-thickness polynomial degree used in the hierarchical modelling of the plate,  $p_z$ , as

$$\tilde{q}_{\Omega^e}|_\gamma = \sum_{i=1}^{p_z+1} \alpha_i \theta_i|_\gamma \quad (4.18)$$

Equation (4.18) is substituted for  $\tilde{q}_{\Omega^e}$  in (4.16), resulting in a system of equations for the unknown coefficients. For the edge  $\gamma_2$ ,

$$\mathbf{M}_{\gamma_2} \boldsymbol{\alpha} = \left\{ \begin{array}{l} F_{\Omega^e}(\theta_1^{\gamma_2}) - B_{\Omega^e}(\hat{u}, \theta_1^{\gamma_2}) - \int_{\gamma_2} \bar{q}_{\Omega^e} \theta_1^{\gamma_2} \, ds - \int_{\gamma_1} q_b \theta_1^{\gamma_2} \, ds \\ F_{\Omega^e}(\theta_2^{\gamma_2}) - B_{\Omega^e}(\hat{u}, \theta_2^{\gamma_2}) - \int_{\gamma_2} \bar{q}_{\Omega^e} \theta_2^{\gamma_2} \, ds - \int_{\gamma_3} q_t \theta_2^{\gamma_2} \, ds \\ F_{\Omega^e}(\theta_3^{\gamma_2}) - B_{\Omega^e}(\hat{u}, \theta_3^{\gamma_2}) - \int_{\gamma_2} \bar{q}_{\Omega^e} \theta_3^{\gamma_2} \, ds \\ \vdots \\ F_{\Omega^e}(\theta_{p_z+1}^{\gamma_2}) - B_{\Omega^e}(\hat{u}, \theta_{p_z+1}^{\gamma_2}) - \int_{\gamma_2} \bar{q}_{\Omega^e} \theta_{p_z+1}^{\gamma_2} \, ds \end{array} \right\} \quad (4.19)$$

For  $\gamma_4$ ,

$$\mathbf{M}_{\gamma_4} \boldsymbol{\alpha} = \left\{ \begin{array}{l} F_{\Omega^e}(\theta_1^{\gamma_4}) - B_{\Omega^e}(\hat{u}, \theta_1^{\gamma_4}) - \int_{\gamma_4} \bar{q}_{\Omega^e} \theta_1^{\gamma_4} ds - \int_{\gamma_1} q_b \theta_1^{\gamma_4} ds \\ F_{\Omega^e}(\theta_2^{\gamma_4}) - B_{\Omega^e}(\hat{u}, \theta_2^{\gamma_4}) - \int_{\gamma_4} \bar{q}_{\Omega^e} \theta_2^{\gamma_4} ds - \int_{\gamma_3} q_t \theta_2^{\gamma_4} ds \\ F_{\Omega^e}(\theta_3^{\gamma_4}) - B_{\Omega^e}(\hat{u}, \theta_3^{\gamma_4}) - \int_{\gamma_4} \bar{q}_{\Omega^e} \theta_3^{\gamma_4} ds \\ \vdots \\ F_{\Omega^e}(\theta_{p_z+1}^{\gamma_4}) - B_{\Omega^e}(\hat{u}, \theta_{p_z+1}^{\gamma_4}) - \int_{\gamma_4} \bar{q}_{\Omega^e} \theta_{p_z+1}^{\gamma_4} ds \end{array} \right\} \quad (4.20)$$

where  $\mathbf{M}_{\gamma_i}$  is a mass matrix along  $\gamma_i$  defined in (3.22). Equations (4.19) and (4.20) are solved for  $\alpha_i$ , which determines the deviation,  $\tilde{q}_{\Omega^e}$ . The solution for  $\tilde{q}_{\Omega^e}$  and the definition for the average flux in (4.15) are substituted into (4.14) to determine the equilibrated flux applied to the interior element boundaries.

### 4.3.3 Multi-Layer Error Indicator

The error function in the error residual problem (4.13) is approximated by using the equilibrated flux method for in the last term. The approximate error function,  $\hat{e}$ , is defined as a linear combination of the basis functions used in the finite element approximation

$$\hat{e} = \sum_{i=0}^{p_x+\sigma} \sum_{j=0}^{p_z+\sigma} \phi_i(x) \hat{\psi}_j(z) b_{ij} \quad (4.21)$$

where  $\sigma \geq 1$ . The definition for  $\hat{e}$  is substituted for  $e$  and (3.26) is substituted for  $v$  in (4.13), creating a system of equations that is written in matrix form:

$$\begin{aligned} B_{\Omega^e}(\hat{e}, \hat{v}) &= F_{\Omega^e}(\hat{v}) - B_{\Omega^e}(\hat{u}, \hat{v}) - \int_{\partial\Omega^e} \hat{q}_{\Omega^e} \hat{v} ds \\ \mathbf{A}_e \mathbf{b} &= \mathbf{F}_e \end{aligned} \quad (4.22)$$

The error indicator for each element is determined using the energy norm of the approximate error function  $\hat{e}$  defined as

$$\varepsilon_{\Omega^e} = \|\hat{e}\|_{\Omega^e} = \sqrt{B_{\Omega^e}(\hat{e}, \hat{e})} = \left[ \int_{\Omega} (\boldsymbol{\kappa} \nabla \hat{e})^T \nabla \hat{e} d\Omega \right]^{\frac{1}{2}} \quad (4.23)$$

The global error indicator is calculated by computing the sum of the squares of the local error indicators

$$\varepsilon = \left[ \sum_{\Omega^e} (\varepsilon_{\Omega^e})^2 \right]^{1/2} \quad (4.24)$$

## 4.4 Numerical Examples

Results are shown for a two-layer plate with length  $L = 2$ , thickness  $d = 1$ , no internal heat generation,  $(k_x)_1 = (k_z)_1 = 1$ ,  $(k_x)_2 = (k_z)_2 = 10$ , and  $\sigma = 1$ , shown in Figure 4.4. The layers are of equal thickness, and the boundary conditions are

$$\begin{aligned} u &= 0 \quad \text{along the edges } x = 0 \text{ and } x = L \\ -k_z \frac{\partial u}{\partial z} &= 0 \quad \text{along } z = -\frac{d}{2} \\ -k_z \frac{\partial u}{\partial z} &= \frac{4q_0 x(L-x)}{L^2} \quad \text{along } z = \frac{d}{2} \end{aligned} \quad (4.25)$$

where  $q_0 = -10$ . The exact solution is an infinite Fourier series defined for each layer

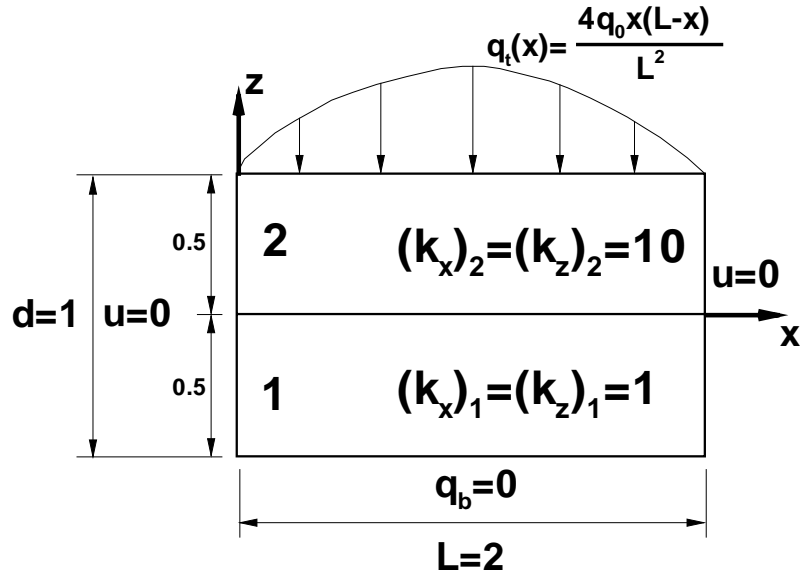


Figure 4.4: Two-dimensional plate with two layers for numerical results.

$$u = \sum_{n=1}^{\infty} \sin\left(\frac{n\pi x}{L}\right) \begin{cases} A_n \sinh(\alpha_n^1 z) + B_n \cosh(\alpha_n^1 z) & -\frac{d}{2} \leq z \leq 0 \\ C_n \sinh(\alpha_n^2 z) + D_n \cosh(\alpha_n^2 z) & 0 \leq z \leq \frac{d}{2} \end{cases} \quad (4.26)$$

where

$$\begin{aligned}
\alpha_n^i &= \frac{n\pi}{L} \sqrt{\frac{(k_x)_i}{(k_z)_i}} \\
A_n &= -\frac{32Lq_0 \tanh\left(\frac{d}{2}\alpha_n^1\right)}{n^4\pi^4 \sqrt{(k_x)_2(k_z)_2} \left[ \sinh\left(\frac{d}{2}\alpha_n^2\right) + \cosh\left(\frac{d}{2}\alpha_n^2\right) \sqrt{\frac{(k_x)_1(k_z)_1}{(k_x)_2(k_z)_2}} \tanh\left(\frac{d}{2}\alpha_n^1\right) \right]} \\
B_n &= \frac{A_n}{\tanh\left(\frac{d}{2}\alpha_n^1\right)} \\
C_n &= A_n \sqrt{\frac{(k_x)_1(k_z)_1}{(k_x)_2(k_z)_2}} \\
D_n &= \frac{A_n}{\tanh\left(\frac{d}{2}\alpha_n^1\right)} \tag{4.27}
\end{aligned}$$

The contours of the exact solution for the plate problem is shown in Figure 4.5.

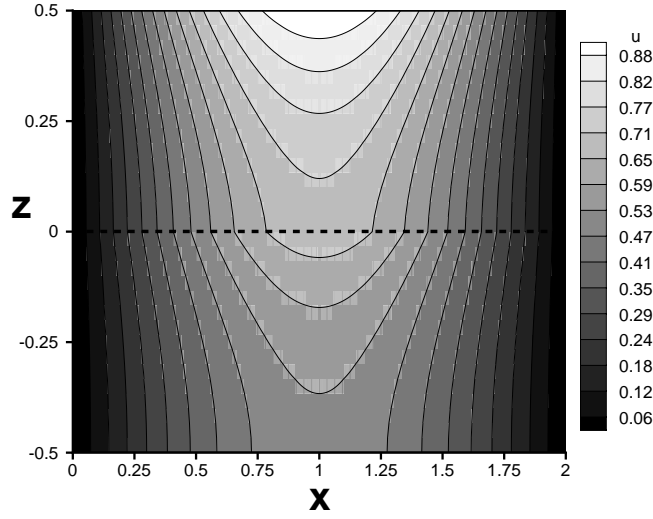


Figure 4.5: Exact solution for the two layer example.

To illustrate the improvement in the accuracy of the finite element solution obtained with the optimal hierarchical model, the actual error obtained using the new through-thickness basis functions is compared with the actual error obtained using the homogenized basis functions in Figure 4.6. Each graph shows the actual error in the energy norm versus the inverse of the mesh size for a fixed value of  $p_x$ . Each line in each graph represents a fixed value of  $p_z$  with uniform mesh refinement. For each

value of  $p_x$ , the results show that the error is less when using the optimal through-thickness basis functions except when  $p_z = 1$ . The rate of convergence of the error is  $p_x$  for the optimal basis functions as seen in the first graph in Figure 4.6. The hierarchical modelling error becomes dominant after only a few mesh refinements when using the single-layer (homogenized) basis functions. The hierarchical modelling error is much larger for the homogenized basis functions than for the optimal ones for the same model order,  $p_z$ . Also, the hierarchical modelling with the homogenized basis functions fails to converge with  $p_z$  as the modelling error does not decrease significantly as  $p_z$  is increased.

The performance of the error estimate for the multi-layer example is shown in Figure 4.7. The comparison of the actual error and the estimated error shows that the error estimate predicts the error in the solution reasonably well.

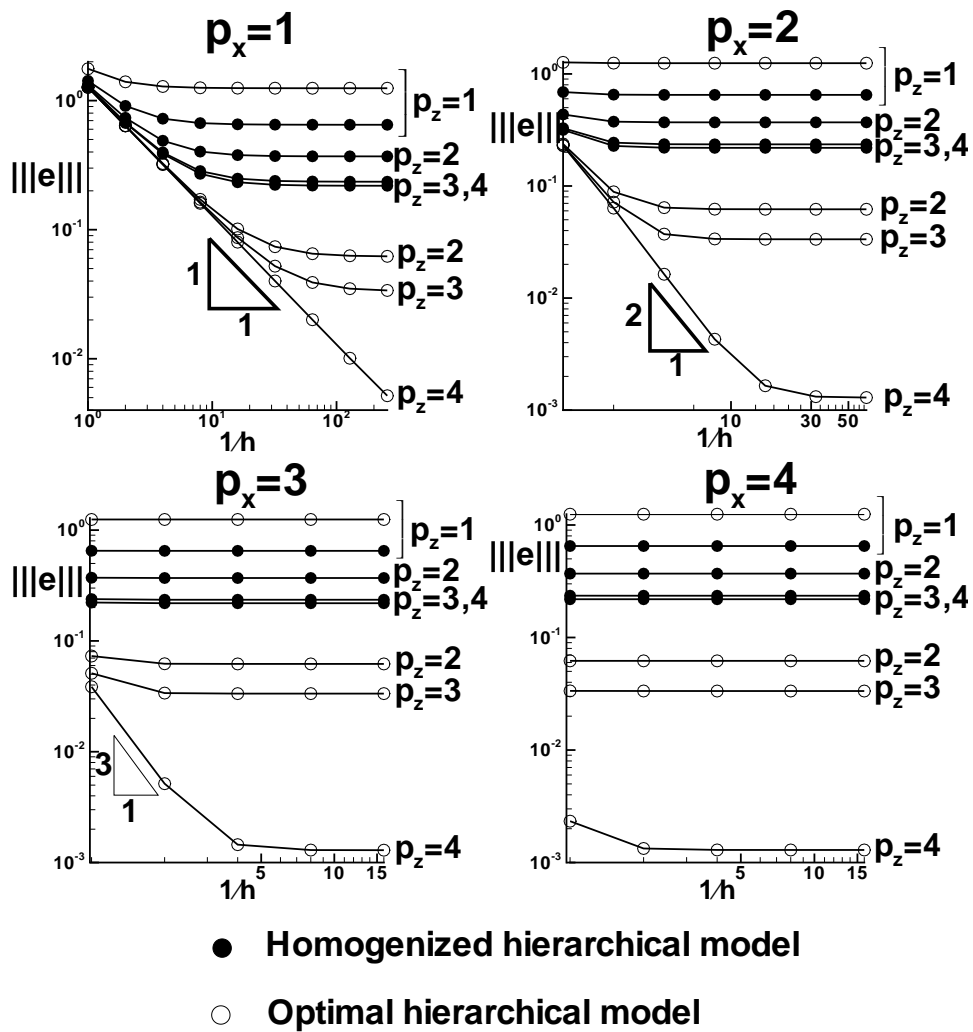


Figure 4.6: Actual error in solutions obtained for two layer example.

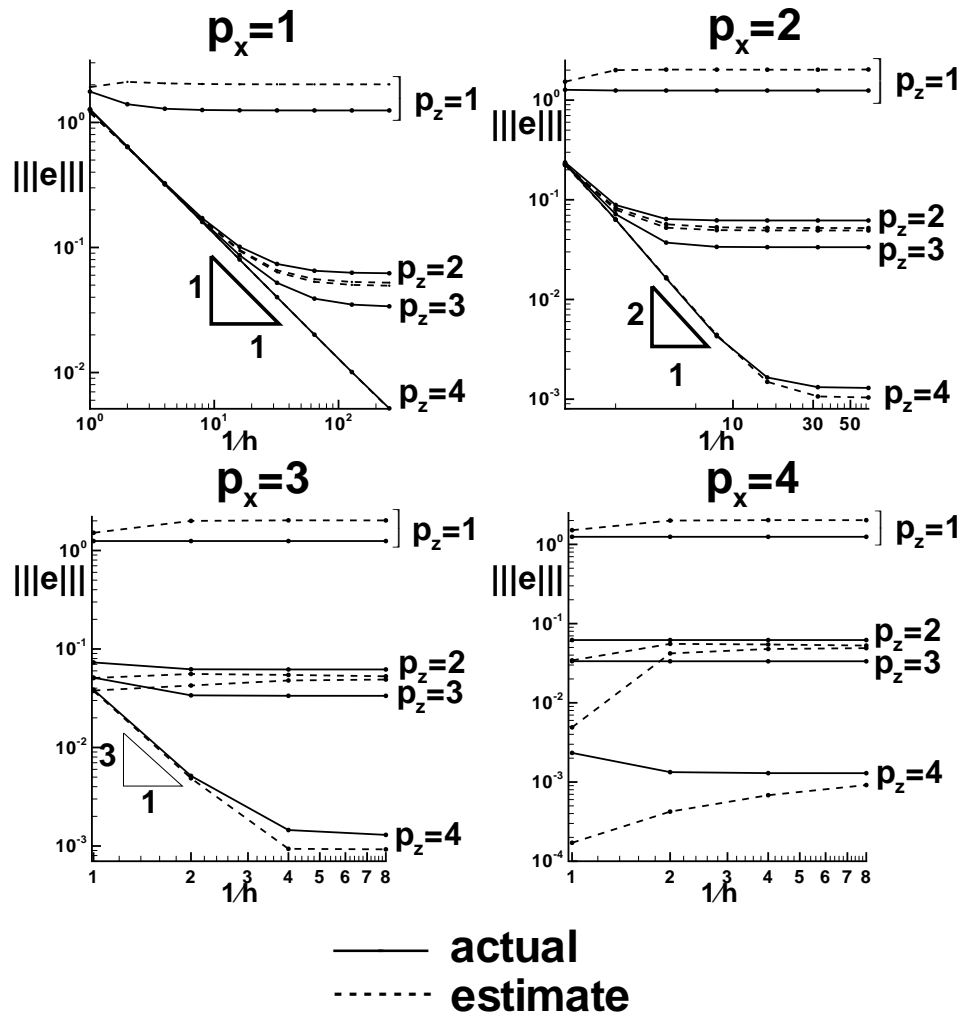


Figure 4.7: Comparison of the actual and estimated error for the two layer example.

# Chapter 5

## Concluding Remarks

An overview of the research presented in this thesis is discussed in this chapter. A summary of the main topics of this paper is first presented followed by the conclusions resulting from this research. Finally, recommendations for future work in this area of research are given.

### 5.1 Summary

Finite element methods are widely used in engineering analysis of many types of problems. Hierarchical modelling combined with p-version finite elements is an advanced method of approximating solutions to a number of engineering problems, and are applied to heat conduction in this work. Error estimation provides a qualitative measure of the accuracy of the finite element solution. *A posteriori* error estimation is necessary for adaptive schemes, where mesh refinement or polynomial enrichment is automatically controlled to efficiently improve the accuracy of the solution. For hierarchical modelling combined with the p-version finite element method, additional information about the error can be determined through the use of directional error indicators, which distinguish between the hierarchical modelling error and the finite element error. Application of *a posteriori* error estimation is important to single-layered as well as multi-layered materials, such as metallic thermal protection

systems and composite laminates. One of the goals of this research is to investigate *a posteriori* error techniques applied to multi-layered materials.

## 5.2 Conclusions

It is shown that a residual based *a posteriori* error estimate method can be effectively applied to a two-dimensional orthotropic material under steady-state conditions. The equilibrated flux method provides more accurate results for the error estimates than the average flux method. Although somewhat more computationally expensive than the average flux method, the accuracy of the results from using the equilibrated flux method are worth the additional effort. The error estimates for this research are determined by performing the analysis on a two-dimensional domain, and while the procedure for three-dimensional domains may be more complex to implement, comparable accuracy is expected. The directional error indicators are shown to provide some insight to separating the error created by the hierarchical model and the finite element method, which will be useful in developing an adaptive scheme. Finally, it is determined that it is necessary to modify the application of the equilibrated flux method to multi-layered materials by using a discontinuous approximate boundary flux to obtain accurate results. One such modification is developed and investigated, and the error estimates are shown to predict the error in the solution reasonably well.

## 5.3 Recommendations

The research presented in this work may be extended in several different ways. The application of this research was limited to two-dimensional steady-state problems. It is recommended that future work include three-dimensional work with hierarchical modelling in the through-thickness direction. Additionally, extension to transient analyses would be the next step. Development of an adaptive scheme using the er-

ror estimates discussed in this research should be investigated. The error estimates provide the information needed to determine when and where a more accurate approximation is needed, and the adaptive scheme can use the error estimates for automatic mesh refinement, p-enrichment, or a combination of both. Finally, for the multi-layered problems, other methods of approximating the heat flux on the element boundary to provide more accurate error estimates should be investigated. One suggested approach is equilibrating the flux on each layer of the element.

# Bibliography

- [1] Ainsworth, M. and Oden, J.T., *A Posteriori Error Estimation in Finite Element Analysis*, John Wiley and Sons, Inc., 2000.
- [2] Babuska, I., Lee, I., and Schwab, C. "On the A-Posteriori Estimation of the Modelling Error for the Heat Conduction in a Plate and Its Use for Adaptive Hierarchical Modelling," *Applied Numerical Mathematics*, Vol. 14, 1994, pp. 5-21.
- [3] Surana, K.S., and Orth, N.J. "Completely Hierarchical p-Version Axisymmetric Shell Element for Nonlinear Heat Conduction in Laminated Composites," *Computers and Structures*, Vol. 46, No. 5, 1993, pp. 777-789.
- [4] Szabó, B. and Babuška, I., *Finite Element Analysis*, John Wiley and Sons, Inc., 1991.
- [5] Vogelius, M., and Babuška, I., "On a Dimensional Reduction Method. I. The Optimal Selection of Basis Functions," *Mathematics of Computations*, Vol. 37, 1981, pp. 31-46.
- [6] Averill, R.C., and Yip, Y.C. "Thick Beam Theory and Finite Element Model with Zig-Zag Sublaminar Approximations," *AIAA Journal*, Vol. 34, No. 8, 1996.

- [7] Babuška, I., and Rheinboldt, W., "Adaptive Approaches and Reliability Estimations in Finite Element Analysis," *Computer Methods in Applied Mechanics and Engineering*, 17/18, 1979, pp. 519-540.
- [8] Babuška, I., Zienkiewicz, O.C., Gago, J., and Oliveira, E.R. de A., *Accuracy Estimates and Adaptive Refinements in Finite Element Computations*, John Wiley and Sons, Ltd., 1986.
- [9] Ladeveze, P., and Leguillon, D. "Error Estimate Procedure in the Finite Element Method and Applications," *SIAM J. Numer. Anal.*, Vol. 20, No. 3, pp. 485-509, 1983.
- [10] Kelly, D.W. "The Self-Equilibration of Residuals and Complementary A Posteriori Error Estimates in the Finite Element Method," *International J. Numer. Methods Engrg.*, Vol. 20, pp. 1491-1506, 1984.
- [11] Bank, R.E., and Weiser, A. "Some A Posteriori Error Estimators for Elliptic Partial Differential Equations," *Mathematics of Computations*, Vol. 44, pp. 283-301, 1985.
- [12] Ainsworth, M. and Oden, J.T. "A Unified Approach to A Posteriori Error Estimation Based On Element Residual Methods," *Numer. Math.*, Vol. 34, No. 1, pp. 228-245, 1997.
- [13] Oden, J.T., and Prudhomme, S. "Goal-Oriented Error Estimation and Adaptivity for the Finite Element Method," *Computers and Mathematics with Applications*, Vol. 41, 2001, pp. 735-756.
- [14] Kreith, F., and Bohn, M.S., *Principles of Heat Transfer*, Sixth Ed., Brooks/Cole, 2001.

- [15] Reddy, J.N., *An Introduction to the Finite Element Method*, McGraw-Hill, 1993.
- [16] Oden, J.T., *Applied Functional Analysis*, Prentice-Hall, Inc. 1979.
- [17] Zwillinger, D., *CRC Standard Mathematic Tables and Formulae*, 30th Ed., CRC Press, Inc. 1996.
- [18] Zienkiewicz, O.C., and Morgan, K., *Finite Elements and Approximation*, John Wiley and Sons, Inc. 1983.
- [19] Chandrapatla, T.R., and Belegundu, A.D., *Introduction to Finite Elements in Engineering*, Prentice-Hall, Inc., 1997.
- [20] Huebner, K.H., Thornton, E.A., and Byrom, T.G., *The Finite Element Method for Engineers*, Third Ed., John Wiley and Sons, Inc. 1995.
- [21] Press, W.H., Teukolsky, S.A., Vetterling, W.T., and Flannery, B.P., *Numerical Recipes in Fortran 77*, Second Ed., Cambridge University Press, 1992.

| REPORT DOCUMENTATION PAGE  |   |  | Form Approved<br>OMB No. 0704-0188                                       |  |
|--|---|--|--|--|
| Public reporting burden for this collection of information is estimated to average 1 hour per response, including the time for reviewing instructions, searching existing data sources, gathering and maintaining the data needed, and completing and reviewing the collection of information. Send comments regarding this burden estimate or any other aspect of this collection of information, including suggestions for reducing this burden, to Washington Headquarters Services, Directorate for Information Operations and Reports, 1215 Jefferson Davis Highway, Suite 1204, Arlington, VA 22202-4302, and to the Office of Management and Budget, Paperwork Reduction Project (0704-0188), Washington, DC 20503.   |   |  |  |  |
| 1. AGENCY USE ONLY (Leave blank)   |   | 2. REPORT DATE<br>November 2002                            | 3. REPORT TYPE AND DATES COVERED<br>Contractor Report                    |  |
| 4. TITLE AND SUBTITLE<br>Finite Element <i>A Posteriori</i> Error Estimation for Heat Conduction   |   |  | 5. FUNDING NUMBERS<br>NCC1-01017<br>706-85-12-01                         |  |
| 6. AUTHOR(S)<br>Christopher G. Lang  |   |  |  |  |
| 7. PERFORMING ORGANIZATION NAME(S) AND ADDRESS(ES)<br>The George Washington University<br>Joint Institute for Advancement of Flight Sciences<br>Langley Research Center<br>Hampton, VA 23681-2199  |   |  | 8. PERFORMING ORGANIZATION<br>REPORT NUMBER                              |  |
| 9. SPONSORING/MONITORING AGENCY NAME(S) AND ADDRESS(ES)<br>National Aeronautics and Space Administration<br>Langley Research Center<br>Hampton, VA 23681-2199  |   |  | 10. SPONSORING/MONITORING<br>AGENCY REPORT NUMBER<br>NASA/CR-2002-211958 |  |
| 11. SUPPLEMENTARY NOTES<br>Langley Technical Monitor: Kim S. Bey<br>The information in this report was offered as a thesis in partial fulfillment of the requirements for the degree of Master of Science, The Goerge Washington University, August 2002   |   |  |  |  |
| 12a. DISTRIBUTION/AVAILABILITY STATEMENT<br>Unclassified-Unlimited<br>Subject Category 64                      Distribution: Nonstandard<br>Availability: NASA CASI (301) 621-0390   |   |  | 12b. DISTRIBUTION CODE   |  |
| 13. ABSTRACT (Maximum 200 words)<br>This research investigates residual-based a posteriori error estimates for finite element approximations of heat conduction in single-layer and multi-layered materials. The finite element approximation, based upon hierarchical modelling combined with p-version finite elements, is described with specific application to a two-dimensional, steady state, heat-conduction problem. Element error indicators are determined by solving an element equation for the error with the element residual as a source, and a global error estimate in the energy norm is computed by collecting the element contributions. Numerical results of the performance of the error estimate are presented by comparisons to the actual error. Two methods are discussed and compared for approximating the element boundary flux. The equilibrated flux method provides more accurate results for estimating the error than the average flux method. The error estimation is applied to multi-layered materials with a modification to the equilibrated flux method to approximate the discontinuous flux along a boundary at the material interfaces. A directional error indicator is developed which distinguishes between the hierarchical modeling error and the finite element error. Numerical results are presented for single-layered materials which show that the directional indicators accurately determine which contribution to the total error dominates. |   |  |  |  |
| 14. SUBJECT TERMS<br>Error estimation; Heat conduction; Hierarchical model; Finite elements;<br>Equilibrated flux; Directional error   |   |  | 15. NUMBER OF PAGES<br>87  |  |
|  |   |  | 16. PRICE CODE   |  |
| 17. SECURITY CLASSIFICATION<br>OF REPORT<br>Unclassified   | 18. SECURITY CLASSIFICATION<br>OF THIS PAGE<br>Unclassified | 19. SECURITY CLASSIFICATION<br>OF ABSTRACT<br>Unclassified | 20. LIMITATION<br>OF ABSTRACT<br>UL                                      |  |